ANNALI DI GEOFISICA, VOL. XXXVII, N. 6, December 1994

Empirical ground motion prediction

Alexei G. Tumarkin and Ralph J. Archuleta
Institute for Crustal Studies, University of California, Santa Barbara, CA, U.S.A.

Abstract
New methods of site-specific ground motion prediction in the time and frequency domains are presented. A large earthquake is simulated as a composite (linear combination) of observed small earthquakes (subevents) assuming Aki-Brune functional models of the source time functions (spectra). Source models incorporate basic scaling relations between source and spectral parameters. Ground motion predictions are consistent with the entire observed seismic spectrum from the lowest to the highest frequencies. These methods are designed to use all the available empirical Green's functions (or any subset of observations) at a site. Thus a prediction is not biased by a single record, and different possible source-receiver paths are taken into account. Directivity is accounted for by adjusting the apparent source duration at each site. Our time-series prediction algorithm is based on determination of a non-uniform distribution of rupture times of subevents. By introducing a specific rupture velocity we avoid the major problem of deficiency of predictions around the main event's corner frequency. A novel notion of partial coherence allows us to sum subevents' amplitude spectra directly without using any information on their rupture times and phase histories. Predictions by this spectral method are not dependent on details of rupture nucleation and propagation, location of asperities and other predominantly phase-affecting factors, responsible for uncertainties in time-domain simulations.

Key words *strong motions – composite earthquakes – synthetics – source spectra*

1. Introduction

How does one predict ground motion for a specific site from a future earthquake? Short of actually predicting an earthquake itself the prediction of the expected ground motion remains one of the most fundamental questions in seismology. This problem consists of two parts: a description of the earthquake and a definition of ground motion.

Any description of an earthquake has inherent uncertainties. Nonetheless years of study of past earthquakes provide gross constraints, *e.g.*, the shape of the seismic spectrum, average rupture velocity, scaling relations between the seismic moment and the source size.

How is ground motion defined? The task of predicting the amplitude and phase of the particle acceleration at all frequencies is an impossible undertaking. Yet a meaningful ground motion prediction must include the full bandwidth of seismic waves. Is a complete time history necessary? Is it possible to obtain meaningful ground motion predictions if we completely neglect phase information?

We study this fundamental problem of seismology by developing new empirical methods of ground motion prediction based on multiple source models (fig. 1). The idea of many empirical Green's functions methods (Hartzell, 1978) is to utilize the observed small earthquakes originating within the rupture area of the simulated large earthquake as its subsources, representing heterogeneities, asperities, etc. For the validity of this approach all subevents should have focal mechanisms similar to that of the simulated main event. Suppose that we have a good coverage of the an-

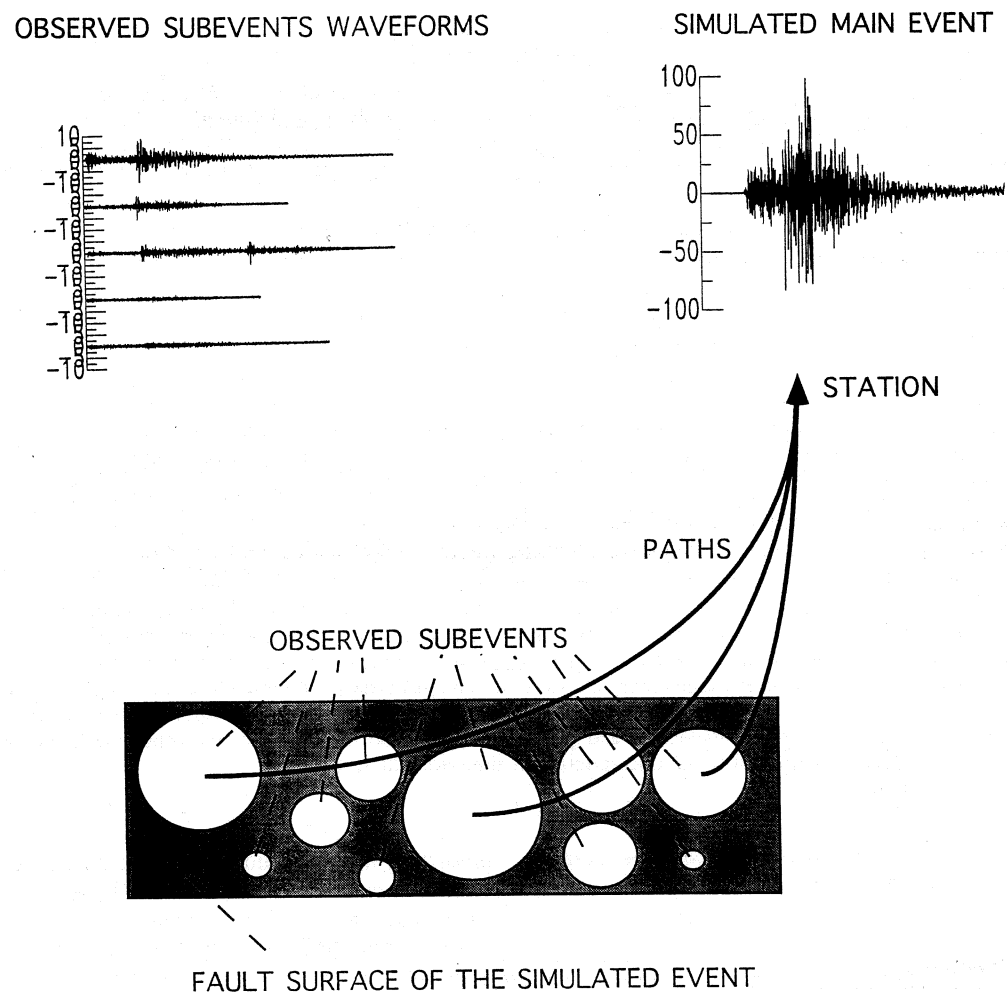

Fig. 1. Schematic diagram of the ground motion prediction with multiple empirical Green's functions. Observed NS-components of ground acceleration from 5 subevents (top left) and from the main shock (top right) are shown.

ticipated main event rupture area by observed subevents. Then we are trying to simulate the large earthquake as a subsequent rupture of properly scaled and lagged subevents. Such procedure will account for the source-receiver geometry by virtue of the initial choice of only those subevents, which are co-located with the main event. Directivity effects can be taken into consideration by determining rupture times of subevents according to both their position on the fault with respect to the main event hypocenter and the azimuth between the site and the direction of rupture propagation.

The important features of our approach are the following:

- it is completely empirical;
- it allows one to use all the available

records at a site. Thus a prediction is not biased by a single record, and different possible source-receiver paths are taken into account;

– it requires the following input parameters for the simulated large event: i) target seismic moment M_0; ii) location of the seismogenic zone, in particular its size R_0; iii) direction of rupture propagation; iv) location of the hypocenter (not required for the spectral prediction method).

There are no other free parameters.

– By applying the method to all three components of ground motion we can predict simultaneously the three components of ground motion at a site.

– It exploits the established connection of the basic scaling relations (Aki, 1967; Brune, 1970; Kanamori and Anderson, 1975) between large and small earthquakes to parameters of the seismic source spectrum. This results in a flexibility of the method with respect to different observed seismic parameters' scaling and spectral falloffs.

– It produces a ground motion prediction in the whole frequency range avoiding deficiency in spectral amplitudes near the target corner frequency.

The paper essentially consists of two parts conventionally called «Time-Series Prediction» and «Spectral Prediction». The principal difference between them is that the time-domain approach requires both the amplitude and phase information to produce time-series predictions, while the spectral approach uses only amplitude spectra of subevents to predict the amplitude spectrum of the target earthquake. On the other hand the time-domain additions of subevents can be equally well performed in the spectral domain by considering simultaneously the amplitude and phase spectra. At the same time our spectral methods are capable of producing time-series by associating either subevents phase information or random phase with the amplitude spectral prediction.

Thus the first part is devoted to methods of adding subevents in the time domain. Any such method requires knowledge (or determination) of rupture times of subevents. In particular, we show that it is possible to perturb rupture velocity in a multiple source model consisting of identical constant stress drop subevents in order to produce an arbitrary target source. The idea of adjusting rupture times of identical subevents was suggested by Wennerberg (1990). However he used a non-causal subevent-to-main event transfer function that resulted in unrealistic negative rupture times on the fault. By using both the amplitude and the phase of the Brune's source spectral model (Dan *et al.*, 1990) we show how the model develops only positive rupture times. As a by-product we find a finite rupture velocity earthquake model with a Brune spectrum.

The second part is the investigation into theoretical principles of ground motion prediction and the novel methodology of construction of source amplitude spectra based on scaling considerations. A new method of empirical spectral prediction, which uses only observed amplitude spectra of small earthquakes co-located with the predicted large earthquake, is developed. This new method does not require the knowledge of details of seismic rupture and is theoretically capable of predicting ground motion spectra in the whole frequency range of analyzed subevents.

The third part shows applications of these ground motion prediction algorithms to data. All of this is followed by a discussion of the methods and their applicability to simulating ground motion from large earthquakes.

1.1. *Empirical Green's functions methods*

The general concept of the Empirical Green's Functions Method (EGFM) is to account for realistic path and site effects by using observed records of the so-called subevents – small earthquakes located within the rupture area of the simulated large earthquake (main event) (fig. 1). The idea of EGFM (Hartzell, 1978; Wu, 1978) was extensively used for synthesizing strong ground motions as well as for inverting for source properties of seismic ruptures (Joyner and Boore, 1988; Aki and Irikura, 1991).

The major and the most difficult part of this approach is deciding how to sum the subevents' records to obtain the prediction (Hartzell, 1978; Irikura, 1983; Joyner and Boore, 1986; Heaton and Hartzell, 1989). We study this problem in both the time and the frequency domains by providing general methods of adding arbitrary sets of observations for site-specific ground motion simulations of scenario earthquakes. A different EGFM approach based on a kinematic modeling of the seismic rupture process (Hutchings, 1994) lies beyond the scope of this paper.

Often, EGFM considers a single observed subevent in order to simulate the ground motions for an anticipated main event. This subevent is replicated many times to obtain a distribution of similar subevents covering the expected rupture area of the main event. Using only one initial record for EGFM allows the predictions to have a strong dependence on characteristics of the input record. Consequently, there is a large variation in predictions simply due to the choice of a subevent (Dan *et al.*, 1990).

In order to match the seismic radiation for both lowest and highest frequencies a subevent's waveform might be appropriately filtered in the time or frequency domains (Irikura, 1983; Boatwright, 1988; Heaton and Hartzell, 1989), or it might be specifically scaled and replicated (Joyner and Boore, 1986). Also, a satisfactory fit in the whole frequency range can be achieved by choosing an appropriate probability distribution of time delays between these identical subevents (Wennerberg, 1990). Another approach is to use EGFM to predict ground motions in a limited frequency range, say, above a certain frequency (Heaton and Hartzell, 1989) and then combine the results with a deterministic modeling at low frequencies (Sommerville, 1993).

Joyner and Boore (1988) were the first to notice another major problem. The common methods that provide a satisfactory simultaneous fit to the lowest and highest frequencies of the target spectrum (Irikura, 1983; Joyner and Boore, 1986; Boatwright, 1988) are all based on a uniform distribution of rupture times of subevents, *i.e.*, a constant rupture velocity over the fault. However this natural assumption leads to a significant underestimation of the main event's spectrum in the vicinity of the target corner frequency. This problem can not be overcome by allowing for different size subevents. In fig. 2a we show simulations of the target Brune's spectrum with $f_0 = 1$ Hz by a fractal distribution of subevents with corner frequencies between 5 Hz and 25 Hz. The underestimation of the target spectrum in the vicinity of the corner frequency is a common feature of both Boatwright's and Joyner-Boore's predictions. This deficit is especially striking when we consider the total kinetic energy. To see this we plot the power spectra of the Brune's velocity pulse and the corresponding simulations from fig. 2a. The Joyner-Boore prediction accounts for only 36% of the target energy; while Boatwright's prediction accounts for only 32% of the energy (fig. 2b).

1.2. *Source time functions and spectra*

Throughout this paper we use a functional description of the *S*-wave radiation that was suggested and verified against observations and physical models in pioneering works of K. Aki and J. Brune (Aki, 1967; Brune, 1970, 1971). The $\omega^{-\gamma}$ spectral model with three parameters: M_0 – the seismic moment of the event, ω_0 – corner frequency (associated with the event's linear dimension and duration), and γ – high-frequency decay rate, has been widely used to study radiation of seismic sources (Joyner and Boore, 1988; Aki and Irikura, 1991). Different functional models of seismic sources (*e.g.*, Randall, 1973) as well as the *P*-wave radiation can be treated along the same lines.

According to the classic ω-squared model (Aki, 1967; Brune, 1970, 1971), it is assumed that the shape of displacement amplitude spectrum $|S(\omega)|$ of a seismic event is

$$|S(\omega)| = C_s \frac{M_0}{1 + \left(\frac{\omega}{\omega_0}\right)^2} \qquad (1.1)$$

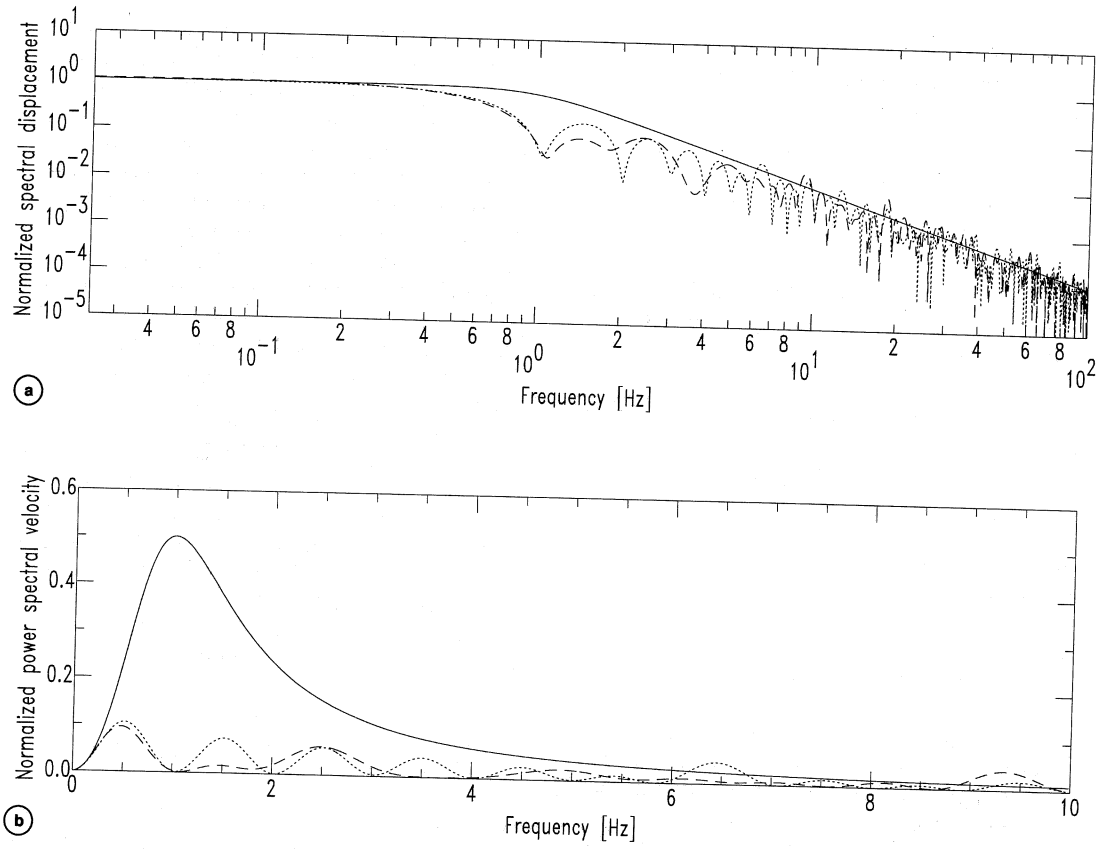

Fig. 2a,b. Simulation of the Brune's spectrum (f_0 = 1 Hz) by a fractal distribution of subevents (D = 2, f_{min} = 5 Hz, f_{max} = 25 Hz) with uniformly distributed rupture times. a) Normalized displacement amplitude spectra. Aki-Brune spectrum (1.1) is a solid line; simulation by our generalization of the Joyner-Boore method developed in the part «Spectral prediction» is plotted as a dotted line; simulation by Boatwright's method (Boatwright, 1988) is a dashed line. b) Normalized velocity power spectra. Note that the uniform distribution of rupture times of subevents produces a local minimum of energy at the target corner frequency for both generalized Joyner-Boore (dotted line) and Boatwright (dashed line) methods. However the $\omega^{-\gamma}$ spectral model (1.5) implies that the source energy (solid line) should be peaked at the corner frequency f_0.

where $\omega = 2\pi f$ is frequency, and C_S is a constant independent of M_0 and ω_0. This amplitude spectrum corresponds to the source time function, known as «Brune's pulse» (Brune, 1970):

$$S(t) = \sqrt{2\pi}\, C_s M_0 \omega_0^2 t e^{-\omega_0 t} \boldsymbol{H}(t) \qquad (1.2)$$

where $\boldsymbol{H}(t)$ is the Heavyside function. The behavior of the Brune's pulse at $t = 0$, *i.e.*, the first-order discontinuity of its derivative, controls the high-frequency behavior of the Aki-Brune's spectrum (1.1) which decays as ω^{-2} (Randall, 1973).

If we consider a more general source time-function

$$S(t) = \frac{\sqrt{2\pi}}{\Gamma(\gamma - 1)} C_s M_0 \omega_0^{\gamma} t^{\gamma - 1} e^{-\omega_0 t} \boldsymbol{H}(t) \qquad (1.3)$$

($\Gamma(\gamma-1)$ is the Gamma-function: $\Gamma(\gamma-1) = (\gamma-2)!$ for integer values of γ), then its Fourier transform has the form:

$$S(\omega) = C_s \frac{M_0}{\left(1 + i\frac{\omega}{\omega_0}\right)^{\gamma}} \qquad (1.4)$$

(for $\gamma = 2$ see Dan *et al.* (1990)); and the corresponding S-wave amplitude spectrum is a familiar $\omega^{-\gamma}$-model

$$|S(\omega)| = C_s \frac{M_0}{\left(1 + \left(\frac{\omega}{\omega_0}\right)^2\right)^{\frac{\gamma}{2}}} \qquad (1.5)$$

in a form considered, for example, by Chael and Kromer (1988).

1.3. *Multiple source models*

It is well known that simple fault models (point-source, double-couple, Haskell-type rupture, etc.) produce accelerograms, that contradict the observed high-frequency complexity of radiated acceleration. There are different ways of introducing heterogeneity into the source models, thus enhancing radiated high frequencies. One of the most promising and widely used methods is to represent a heterogeneous rupture (main event) as a multiple source, *i.e.*, as a composite of discrete subsources (subevents). These multiple source earthquake models include various self-similar models of complex earthquake rupture (Boatwright, 1988), the specific barrier model of Papageorgiou and Aki (1983), as well as some empirical Green's functions methods (Joyner and Boore, 1988). In a general sense every finite-element (or any other discrete) model of a seismic rupture can be viewed as a multiple source model, although often the term «composite earthquake» is reserved for the specific case when each subevent is a small earthquake by itself (Frankel, 1991; Zeng *et al.*, 1994). Such composite earthquake models have inherent limitations (Tumarkin *et al.*, 1994).

At the same time site-specific predictions of ground motions should utilize all the available information contained in observations of earthquakes at the particular site. Uncertainties in the predicted path and site effects can be reduced by examining data from past earthquakes that originate within the rupture area of the anticipated large earthquake (*e.g.*, Joyner and Boore, 1988). If more subevents are simultaneously included as a basis for a prediction, the results are less dependent on characteristics unique to a single seismic record.

Suppose that we have observations of N earthquakes (subevents) having the same focal mechanism and all located within the rupture area of an anticipated large earthquake. The most natural and simple idea is to simulate the radiation from the large earthquake as a linear combination of subsources – scaled and lagged small earthquakes (Heaton and Hartzell, 1989). The source time function $S_0(t)$ of the simulated earthquake is represented as a linear combination of source time functions $S_j(t)$ of subevents:

$$S_0(t) = \sigma_1 S_1(t-\tau_1) + \sigma_2 S_2(t-\tau_2) + \ldots + \sigma_N S_N(t-\tau_N) \qquad (1.6)$$

where τ_j denotes the rupture time of the jth subevent, and σ_j are scaling coefficients for the jth source $S_j(t)$. Allowing for σ_j to be free parameters of the model means that we are permitting arbitrary changes of stress drops of subevents in order to fit the target earthquake (variable stress drop model). Similarly variations of τ_j result in a variable rupture velocity over the fault plane.

Assuming that the source time functions S_0, S_1, ..., S_N have the functional form (1.3), we can rewrite (1.6) as:

$$M_0 \omega_0^{\gamma} t^{\gamma-1} e^{-\omega_0 t} \boldsymbol{H}(t) \approx$$
$$\approx \sigma_1 M_{01} \omega_1^{\gamma} (t-\tau_1)^{\gamma-1} e^{-\omega_1 (t-\tau_1)} \boldsymbol{H}(t-\tau_1) +$$
$$\sigma_2 M_{02} \omega_2^{\gamma} (t-\tau_2)^{\gamma-1} e^{-\omega_2 (t-\tau_2)} \boldsymbol{H}(t-\tau_2) + \ldots +$$
$$\sigma_N M_{0N} \omega_N^{\gamma} (t-\tau_N)^{\gamma-1} e^{-\omega_N (t-\tau_N)} \boldsymbol{H}(t-\tau_N) \qquad (1.7)$$

where M_0, M_{01}, ..., M_{0N} are the seismic moments of the target event and subevents; ω_0, ω_1, ..., ω_N are their corner frequencies; and γ is the common spectral falloff.

Parameters σ_j and τ_j can be determined as solutions of a non-linear least-squares problem (1.7). It is possible to consider a minimization problem with constraints on values of σ_j and τ_j forcing them to lie within the physical limits on stress drops and rupture velocity. If the rupture times τ_j of subevents are postulated (*e.g.*, by assuming a constant rupture velocity), then the coefficients σ_j can be found as a solution of a linear least squares problem. However the problem of determining the best fitting rupture times τ_j is severely non-linear. Nonetheless there is a way of explicitly resolving for τ_j in the framework of the approach proposed by Wennerberg (1990), which is developed in the next section. The relation (1.7) is satisfied by varying only τ_j while keeping σ_j = const. This approach corresponds to a constant stress drop model with a variable rupture velocity.

If the coefficients σ_j and τ_j are found from the relation (1.7), the ground motion $U_0(t)$ from the large earthquake at any site can be approximated as the linear combination of observed ground motions $U_j(t)$ from the subevents:

$$U_0(t) \approx \sigma_1 U_1(t-\tau_1) + \sigma_2 U_2(t-\tau_2) + \ldots + \sigma_N U_N(t-\tau_N) \tag{1.8}$$

which follows from (1.6) and the representation theorem for seismic sources (Aki and Richards, 1980).

1.4. *Directivity*

Radiation from extended seismic sources often has a distinct asymmetric structure. At the same distance from the seismogenic area in the direction of the rupture propagation higher amplitudes are accompanied by shorter durations, while in the back-azimuth lower amplitudes and long durations are observed. This effect was discovered by Benioff (1955) and was named «directivity» by Ben-Menahem (1961). Directivity is closely related to the Doppler effect (Douglas *et al.*, 1988). Earlier theoretical and laboratory studies (Archuleta and Brune, 1975; Boore and Joyner, 1978) as well as observations of moderate and large earthquakes (*e.g.*, Boatwright and Boore, 1982; Kanamori *et al.*, 1992) emphasize the importance of accounting for rupture directivity in ground motion prediction algorithms.

The apparent *S*-wave spectrum $S_\theta(\omega)$ of a seismic source moving with constant speed v observed at a site located at an angle θ from the direction of rupture is given by:

$$S_\theta(\omega) = S\left(\frac{\omega}{D}\right), \tag{1.9}$$

where D is the directivity factor:

$$D = \frac{1}{1 - \frac{v}{\beta}\cos\theta}$$

(Aki and Richards, 1980; Douglas *et al.*, 1988; Joyner, 1991). Thus the directivity factor D is controlled by both the azimuth θ and the Mach number $M = v/\beta$, where β is the shear wave velocity. Directivity effects increase with an increase of the Mach number M.

Assuming the Aki-Brune spectral source model the relation (1.9) is equivalent to the shift of the apparent source corner frequency $\omega_{0\theta}$:

$$\omega_{0\theta} = \frac{\omega_0}{1 - \frac{v}{\beta}\cos\theta}. \tag{1.10}$$

Assuming that $v = 0.85\,\beta$ (Kostrov, 1964; see also below), we find that the apparent source corner frequency is greatly augmented in the forward direction – $\omega_{0\theta} = 6.67\,\omega_0$, $\theta = 0$; unchanged in the direction perpendicular to the fault – $\omega_{0\theta} = \omega_0$, $\theta = 90°$; and reduced by almost a factor of 2 in the back azimuth – $\omega_{0\theta} = 0.54\,\omega_0$, $\theta = 180°$. This angular variation of corner frequency explains the focusing of seismic energy in the direction of rupture prop-

agation. Consequently directivity results in a dramatic azimuthal dependence of the shape of ground motion spectrum and the total radiated energy for unilateral seismic ruptures (Boore and Joyner, 1978; Boatwright and Boore, 1982; Kanamori *et al.*, 1992). It is worth noting that heterogeneous ruptures (and thus multiple source models) may have even stronger directivity effects than uniform ruptures (Boore and Joyner, 1978; Joyner, 1991).

2. Time-series prediction

First we consider an elegant, though particular, approach to solution of the problem (1.6), initiated by Wennerberg (1990). The Brune's source time function (1.2) is approximated by adjusting rupture times but not the stress drops of subevents. The general case (1.3) is treated analogously, but explicit expressions for the rupture velocity (see below) can be obtained only for particular values of γ, such as $\gamma = 3$.

The final result is an algorithm for time-series prediction that allows for an arbitrary number of observed empirical Green's functions.

2.1. *Methods based on an appropriate choice of time delays between subevents*

A number of studies (Irikura, 1983; Joyner and Boore, 1986; Boatwright, 1988; Heaton and Hartzell, 1989) proposed methods for adding identical subevents with uniformly distributed rupture times. These methods succeeded in matching both the low- and high-frequency radiation from simulated earthquakes. At the same time Joyner and Boore (1986, 1988) found that their procedure resulted in a deficit of energy in the intermediate frequency range of the simulated spectrum (especially, in the vicinity of the corner frequency ω_0 of the main event). This fact is an inherent feature of all methods assuming a uniform distribution of rupture times of subevents, *i.e.*, a constant rupture velocity (Joyner and Boore, 1988) (fig. 2a,b). The underestimation of the energy poses the problem of how to lag small earthquakes, other than uniformly distributing their rupture times, in order to simulate radiation from a large earthquake for the whole frequency range.

The importance of an adequate fit to the target spectrum in the vicinity of the corner frequency ω_0 is driven by both seismological and engineering applications of EGFM. The spectral corner frequency ω_0 acts as a resonant frequency of the source energy since the velocity amplitude spectrum of a seismic source is peaked at ω_0 for the common ω-squared model (Aki, 1967; Brune, 1970, 1971). Therefore any misfit to the target spectrum in the vicinity of its corner frequency severely affects the total energy as seen in fig. 2b.

Wennerberg (1990) suggested an approach to eliminate this deficit by determining an appropriate distribution of rupture times of subevents. Wennerberg assumed that the phase spectrum between a small and a large earthquake is preserved. That assumption results in a non-causal transfer function for small-to-large earthquake scaling leading to unrealistic negative rupture times for one half of the subevents (fig. 3).

In the following section we eliminate the negative rupture times in the Wennerberg's method by using the complex form of the Aki-Brune's spectral model (1.4). Rather than treating the distribution of rupture times of subevents as some transformation of a uniformly distributed random variable (Wennerberg, 1990), we consider rupture time as a function of the position on the fault. This will allow us to study the rupture front velocity in this model and to propose non-instantaneous kinematic source models with Brune-type spectra.

2.2. *Model*

We start from a single small event $S_e(t)$ with seismic moment M_{0e} and corner frequency ω_{0e}. The simulated main event has a seismic moment M_0 and corner frequency ω_0. The fault plane of the large event is uniformly covered by N subevents $S_j(t) = \sigma_j S_e(t - \tau_j)$ ordered according to their distances R_j to the hypocenter

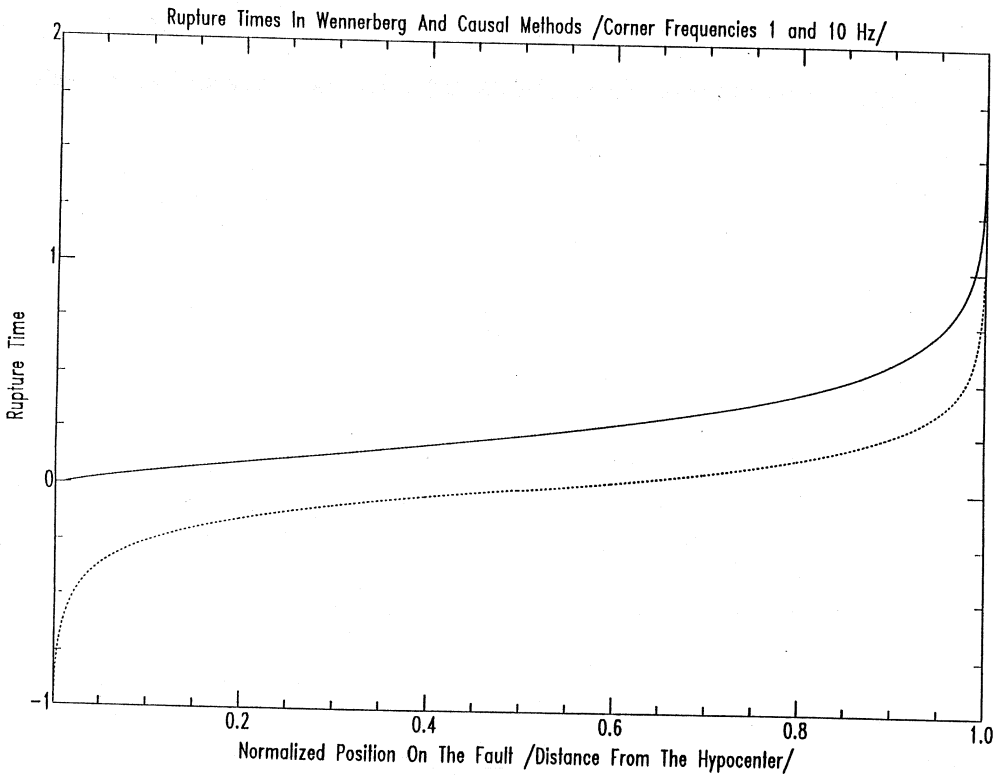

Fig. 3. Rupture time as a function of the position on the fault in Wennerberg's (dotted line) and the causal (eq. (2.7)) (solid line) models. We use the values $f_0 = 1$ Hz and $f_{0e} = 10$ Hz.

of the main event. Each subevent starts radiating at a rupture time τ_j, $j = 1, ..., N$. We denote the seismic moment ratio by ξ: $\xi = M_0/M_{0e}$. The constants σ_j represent the variation of seismic moments (or stress drops) of subevents. Using the condition that the cumulative seismic moment of N subevents matches the target seismic moment, $\sigma_1 + \sigma_2 + \ldots + \sigma_N = \xi$.

We determine rupture times τ_j, such that the resulting source time function

$$S(t) = \sigma_1 S_e(t - \tau_1) + \sigma_2 S_e(t - \tau_2) + \ldots + \sigma_N S_e(t - \tau_N) \tag{2.1}$$

has the Brune's functional form (1.2). The Fourier transform of (2.1) is:

$$S(\omega) = \{\sigma_1 e^{-i\omega\tau_1} + \sigma_2 e^{-i\omega\tau_2} + \ldots + \sigma_N e^{-i\omega\tau_N}\} S_e(\omega) . \tag{2.2}$$

We first consider a continuous rupture process, *i.e.*, a continuous distribution of rupture times of subevents. For a unilaterally propagating rupture (fig. 4a) we introduce a normalized coordinate ρ on the fault as the distance from the hypocenter divided by the total length of rupture R_0. The time of rupture τ will be a function $(\tau)\ \rho$ of the position on the fault; the inverse function $(\rho)\ \tau$ will determine the position of rupture at any time τ.

Let $\sigma_j = \xi\, \tilde{\sigma}_j\, (\rho_j - \rho_{j-1})$, where $(\rho_j - \rho_{j-1})$, is a normalized distance between consecutive subevents. We notice that the expression inside

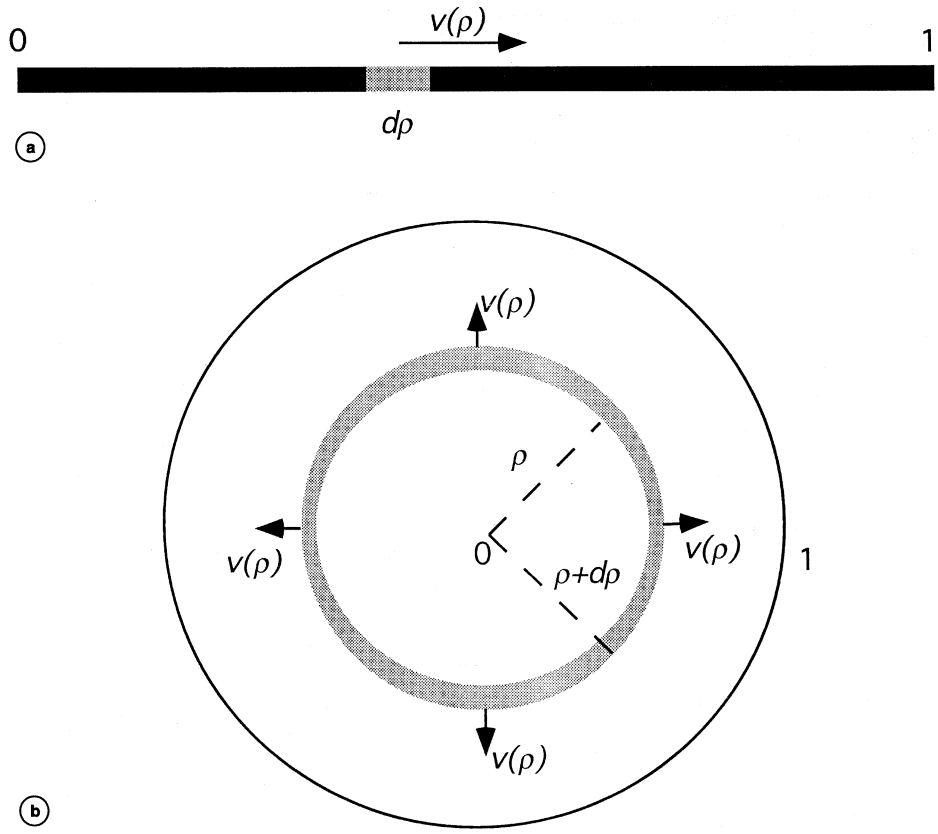

Fig. 4a,b. a) Linear propagating rupture; b) circular expanding rupture.

the brackets in relation (2.2) represents an integral sum for the function $\xi\tilde{\sigma}(\rho)\exp(-i\omega\tau(\rho))$. The function $\tilde{\sigma}(\rho)$ is the density of the seismic moment release on the fault. Then by letting $N \to \infty$, eq. (2.2) becomes

$$\frac{S(\omega)}{S_e(\omega)} = \xi \int_0^1 e^{-i\omega\tau(\rho)}\,\tilde{\sigma}(\rho)d\rho = \\ = \xi \int_0^\infty e^{-i\omega\tau}\,\tilde{\sigma}(\rho(\tau))\rho'(\tau)d\tau\,. \tag{2.3}$$

If we denote the small-to-large earthquake transfer function by $P(\omega)$,

$$P(\omega;\omega_0,\omega_{0e}) = \frac{1}{\sqrt{2\pi}}\,\frac{1}{\xi}\,\frac{S(\omega)}{S_e(\omega)} \tag{2.4}$$

from (2.3) we conclude that $P(\omega)$ is the Fourier transform of the function $\tilde{\sigma}(\rho(t))\rho'(t)$, thus $\tilde{\sigma}(\rho(t))\rho'(t) = P(t;\omega_0,\omega_{0e})$.

For the spectral model (1.4), accounting both for the amplitude and the phase spectra,

$$P(\omega;\omega_0,\omega_{0e}) = \frac{1}{\sqrt{2\pi}}\,\frac{\left(1+i\dfrac{\omega}{\omega_{0e}}\right)^2}{\left(1+i\dfrac{\omega}{\omega_0}\right)^2}\,. \tag{2.5}$$

The behavior of the transfer function (2.5) at high frequencies controls the regularity of its inverse Fourier transform. Since $P(\omega)$ tends to a finite limit at infinity, the function $\tilde{\sigma}(\rho(t))\rho'(t)$ should have a δ-like singularity which can be assigned either to the seismic moment release density $\tilde{\sigma}(\rho)$, or to the rupture velocity $\rho'(t)$ (Madariaga, personal communication). Here we consider the latter case.

Wennerberg (1990) assumed that the phase spectra of a large and a small earthquakes are the same. Thus his transfer function was non-causal, being proportional to the ratio of Brune's amplitude spectra:

$$P(\omega;\omega_0,\omega_{0e}) = \frac{1}{\sqrt{2\pi}} \frac{1+\left(\frac{\omega}{\omega_{0e}}\right)^2}{1+\left(\frac{\omega}{\omega_0}\right)^2}$$

(obtained in (Wennerberg, 1990) by a different argument).

The inverse Fourier transform of (2.5) is

$$P(t,\omega_0,\omega_{0e}) =$$

$$\left(\frac{\omega_0}{\omega_{0e}}\right)^2 \left(\delta(t) + \left[2(\omega_{0e}-\omega_0) + (\omega_{0e}-\omega_0)^2 t\right] e^{-\omega_0 t} \boldsymbol{H}(t)\right) \tag{2.6}$$

If all subevents have the same normalization, $\sigma_j = \xi/N$. Let $\xi = c_\xi (\omega_{0e}/\omega_0)^3$, where the quantity c_ξ describes the deviation from a constant stress drop scaling. To simplify the following calculations we first normalize the original subevent's source time function $S_e(t)$ by c_ξ. Then the function $\tilde{\sigma}(\rho(t)) \equiv 1$, *i.e.*, the seismic moment is uniformly released over the whole fault. Consequently in the case of the linear rupture the normalized rupture velocity $\rho'(t)$ is given by eq. (2.6). The normalized position $\rho(t)$ on the fault at each time moment can be obtained by integrating (2.6):

$$\rho(t,\omega_0,\omega_{0e}) =$$

$$\left\{1 - \left[1 - \left(\frac{\omega_0}{\omega_{0e}}\right)^2 + \left(1 - \frac{\omega_0}{\omega_{0e}}\right)^2 \omega_0 t\right] e^{-\omega_0 t}\right\} \boldsymbol{H}(t). \tag{2.7}$$

By inverting the function $\rho(t)$ from (2.7) we can determine the rupture time $t(\rho)$ for each position ρ on the fault to satisfy the small-to-large earthquake transfer function $P(\omega)$ in (2.4). We compare rupture times from Wennerberg's model and our model (2.7) in fig. 3. We have used the values $f_0 = 1$ Hz and $f_{0e} = 10$ Hz for both models.

Thus Brune's source with the corner frequency ω_0 can be simulated from any number N of subevents with the corner frequency ω_{0e} by the following steps:

1) uniformly distribute N subevents over the linear fault plane (fig. 4a), *i.e.* determine their normalized coordinates ρ_j;

2) determine their rupture times τ_j by inverting (2.7) for τ_j corresponding to given values of ρ_j;

3) add subevents according to (2.1), where $\sigma_j = \xi/N$.

Note that according to (2.7) the position ρ of the subevent on the fault uniquely determines its rupture time $\tau(\rho)$. The quality of the fit increases with an increase of the number of summands N since the rupture times in (2.7) were obtained under the assumption that $N = \infty$.

In fig. 5 we compare our simulations of the Brune's spectrum with $f_0 = 1$ Hz to the Wennerberg's original method (1990) for three values of the subevent's corner frequency $f_{0e} = 3$; 5; 10 Hz. The quality of fits is about the same with slightly less variation in our predictions. We see that this method is capable of producing a satisfactory prediction of spectral amplitudes throughout the entire frequency range.

2.3. *Circular rupture model*

We can extend this approach from 1-D to 2-D for the particular case of a circular rupture

Simulation of Brune's spectrum with f_0 = 1 Hz by adding subevents with f_e= 3,5,10 Hz: Wennerberg's zero-phase distribution for rupture times of subevents

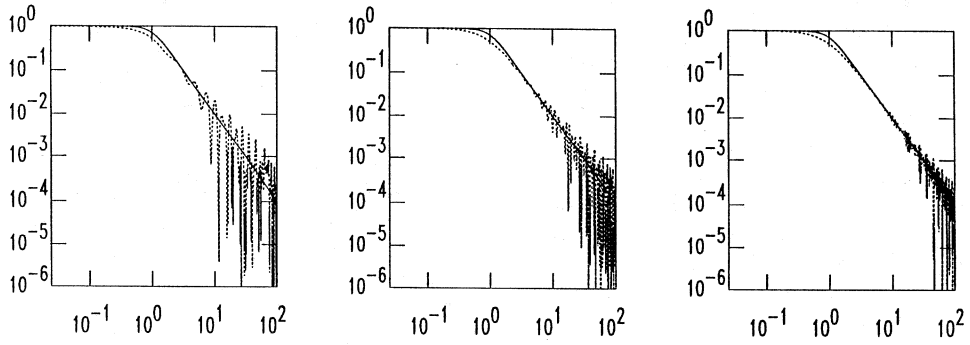

Simulation of Brune's spectrum with f_0 = 1 Hz by adding subevents with f_e= 3,5,10 Hz: Causal distribution for rupture times of subevents

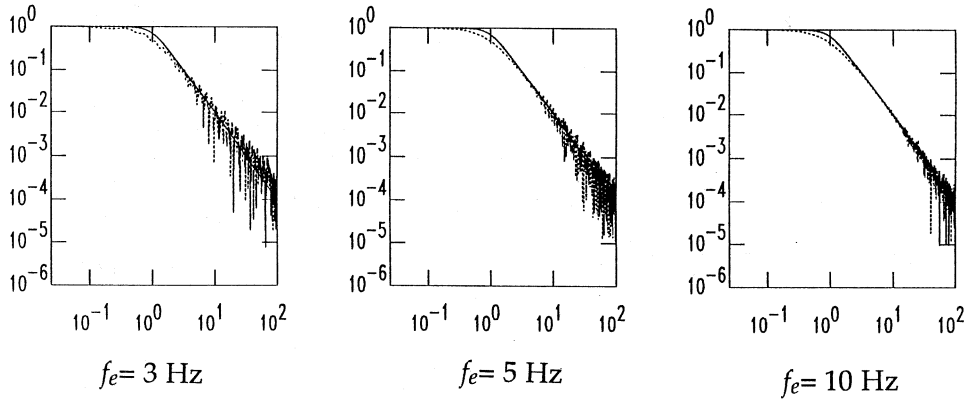

Fig. 5. Simulations of the Brune's spectrum with f_0 = 1 Hz by Wennerberg's (first row) and causal methods (linear rupture case) (second row). We used three values of f_{0e} = 3; 5; 10 Hz. The number N of subevents was chosen to be equal to the seismic moment ratio $N = \left(\frac{\omega_{0e}}{\omega_0}\right)^3$.

model. In an expanding circular rupture (fig. 4b), the elemental length $d\rho$ in (2.3) becomes an elemental annular area $d(\rho^2)$:

$$\frac{S(\omega)}{S_e(\omega)} = \xi \int_0^1 e^{-i\omega\tau(\rho)}\, \tilde{\sigma}(\rho) 2\rho d\rho \,. \qquad (2.8)$$

The normalized radial position of the rupture front for a fault plane consisting of identical stress drop subevents ($\tilde{\sigma}(\rho(t)) \equiv 1$) is given by:

$$\rho(t,\, \omega_0,\, \omega_{0e}) = \sqrt{1 - \left[1 - \left(\frac{\omega_0}{\omega_{0e}}\right)^2 + \left(1 - \frac{\omega_0}{\omega_{0e}}\right)^2 \omega_0 t\right] e^{-\omega_0 t} \boldsymbol{H}(t)} \qquad (2.9)$$

We determine the normalized rupture velocity $\rho'(t)$ by differentiating (2.9):

$$\rho'(t, \omega_0, \omega_{0e}) = \frac{\left(\frac{\omega_0}{\omega_{0e}}\right)^2 \left(\delta(t) + \left[2(\omega_{0e} - \omega_0) + (\omega_{0e} - \omega_0)^2 t\right] e^{-\omega_0 t} \boldsymbol{H}(t)\right)}{2\sqrt{1 - \left[1 - \left(\frac{\omega_0}{\omega_{0e}}\right)^2 + \omega_0 \left(1 - \frac{\omega_0}{\omega_{0e}}\right)^2 t\right] e^{-\omega_0 t}}} \tag{2.10}$$

The rupture velocity $v(t)$ can be obtained from the normalized velocity $\rho'(t)$ using the definition of the normalized coordinate $\rho = r/R_0$ and Brune's relation between the size of the fault R_0, shear wave velocity β, and the S-wave corner frequency ω_0

$$\omega_0 = \frac{2.34\,\beta}{R_0}$$

(Brune, 1970, 1971). Thus

$$v(t) = R_0 \rho'(t) = \frac{2.34\,\beta}{\omega_0} \rho'(t).$$

For a circular expanding rupture of subevents with corner frequency ω_{0e}

$$v(t) = \frac{2.34\beta}{\omega_0} \cdot \frac{\left(\frac{\omega_0}{\omega_{0e}}\right)^2 \left(\delta(t) + \left[2(\omega_{0e} - \omega_0) + (\omega_{0e} - \omega_0)^2 t\right] e^{-\omega_0 t} \boldsymbol{H}(t)\right)}{2\sqrt{1 - \left[1 - \left(\frac{\omega_0}{\omega_{0e}}\right)^2 + \omega_0 \left(1 - \frac{\omega_0}{\omega_{0e}}\right)^2 t\right] e^{-\omega_0 t}}}$$

In the limiting case of $\omega_{0e} = \infty$, *i.e.*, the size of the subevent becoming infinitely small, we find

$$v(t) = \frac{1.17\,\beta\omega_0 t e^{-\omega_0 t}}{\sqrt{1 - [1 + \omega_0 t] e^{-\omega_0 t}}} \boldsymbol{H}(t). \tag{2.11}$$

From (2.11) we see that the rupture velocity in this model (fig. 6) has the following features:

– velocity is a monotonically decreasing function of time (hypocentral distance);
– the maximum value of the rupture velocity is at $t = 0$: $v_{\max} = 1.17\sqrt{2}\beta \approx 1.65\beta$;
– the average value of the rupture front velocity is 0.85 β:

$$v_{\text{ave}} = \int_0^1 v(\rho) d\rho = \int_0^\infty v(t) \rho'(t) dt =$$

$$= \frac{2.34\beta}{\omega_0} \int_0^\infty [\rho'(t)]^2 dt =$$

$$= \frac{2.34\beta}{\omega_0} \int_0^\infty \frac{\omega_0^4 t^2 e^{-2\omega_0 t}}{4(1 - [1 + \omega_0 t] e^{-\omega_0 t})} dt =$$

$$= \frac{2.34\beta}{4} \int_0^\infty \frac{\tau^2 e^{-2\tau}}{1 - [1 + \tau] e^{-\tau}} d\tau$$

with $\tau = \omega_0 t$ and numerically evaluating the integral.

2.4. *Fault composed of Boatwright's asperities*

Boatwright (1988) proposed a composite faulting model where subevents had two characteristic linear dimensions, *i.e.*, two corner frequencies – ω_{0e} related to the size of the subevent, and ω_0 related to the size of the whole fault. Thus Boatwright's asperity for the constant stress drop seismic moment scaling

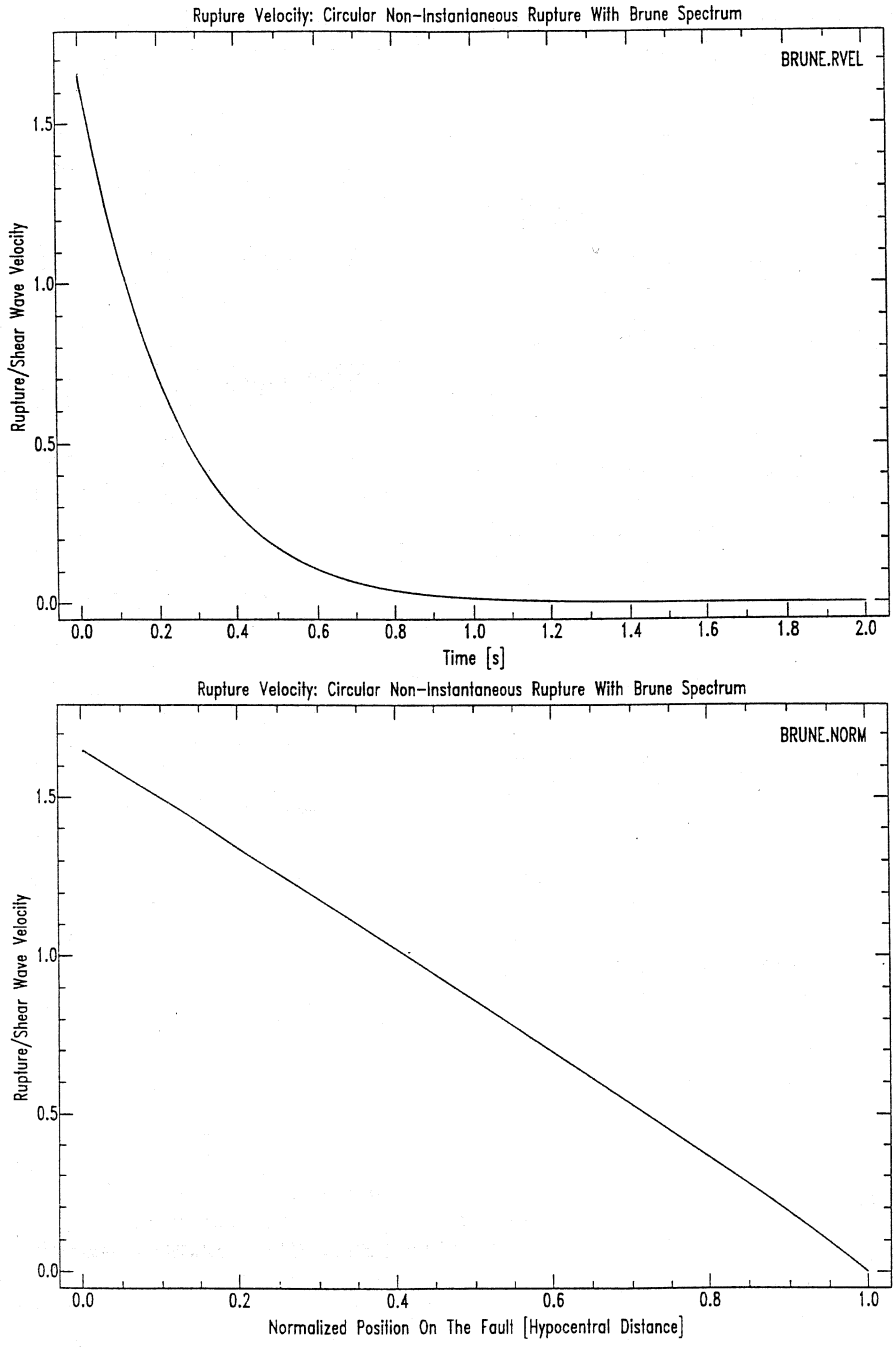

Fig. 6. Rupture velocity for the circular rupture model in the limit case $\omega_{0e} = \infty$, (eq. (2.11)), as a function of time (upper plot) and the position on the fault (lower plot). We plot rupture velocity normalized by the shear wave velocity β.

has a spectrum of the form:

$$u_a(\omega) \propto \frac{1}{\omega_{0e}(\omega_0 + i\omega)(\omega_{0e} + i\omega)} . \quad (2.12)$$

Therefore, the asperity-to-large earthquake transfer function in his case is

$$P(\omega;\ \omega_0,\ \omega_{0e}) = \frac{1}{\sqrt{2\pi}} \frac{1 + i\frac{\omega}{\omega_{0e}}}{1 + i\frac{\omega}{\omega_0}} . \quad (2.13)$$

The inverse Fourier transform of (2.13) is

$$P(t,\ \omega_0,\ \omega_{0e}) = \frac{\omega_0}{\omega_{0e}}\left(\delta(t) + (\omega_{0e} - \omega_0)e^{-\omega_0 t}\boldsymbol{H}(t)\right) . \quad (2.14)$$

As in the case of the Brune's crack subevent, eq. (2.14) gives us the normalized rupture velocity $\rho'(t)$ for a linear fault consisting of asperities. The normalized position $\rho(t)$ on the fault at each time moment is obtained by integrating (2.14):

$$\rho(t,\ \omega_0,\ \omega_{0e}) = \left[1 - \left(1 - \frac{\omega_0}{\omega_{0e}}\right)e^{-\omega_0 t}\right]\boldsymbol{H}(t). \quad (2.15)$$

At the initial moment $t = 0$ there is an instantaneous rupture over a fraction of the fault with length

$$\left(\frac{\omega_0}{\omega_{0e}}\right)R_0 ,$$

while in section 2.2. the fraction was given by

$$\left(\frac{\omega_0}{\omega_{0e}}\right)^2 R_0 .$$

Simulation of Brune's source with corner frequency ω_0 using Boatwright's asperities has the following steps:

1) filter the observed small earthquake having a corner frequency ω_{0e} with the earthquake-to-asperity filter to produce the asperity-type source spectrum (2.12) for subevents;

2) uniformly distribute N subevents over a linear fault (fig. 3a), *i.e.*, determine their normalized coordinates ρ_j;

3) determine subevent rupture times by inverting (2.15) for τ_j that correspond to given values of ρ_j;

$$\tau_j = -\frac{1}{\omega_0}\ln\left(\frac{1 - \rho_j}{1 - \frac{\omega_0}{\omega_{0e}}}\right)$$

4) add subevents according to (2.1), where $\sigma_j = \xi/N$.

This 1-D asperity model can be extended to a circular rupture in a manner similar to that given above. The position on the fault is:

$$\rho(t,\ \omega_0,\ \omega_{0e}) = \sqrt{1 - \left(1 - \frac{\omega_0}{\omega_{0e}}\right)e^{-\omega_0 t}\boldsymbol{H}(t)} \quad (2.16)$$

and the normalized rupture velocity $\rho'(t)$ is:

$$\rho'(t,\ \omega_0\ \omega_{0e}) = \frac{\frac{\omega_0}{\omega_{0e}}\left(\delta(t) + (\omega_{0e} - \omega_0)e^{-\omega_0 t}\right)\boldsymbol{H}(t)}{2\sqrt{1 - \left(1 - \frac{\omega_0}{\omega_{0e}}\right)e^{-\omega_0 t}}}$$

If the asperity becomes infinitely small $\omega_{0e} \gg \omega_0$, then the rupture front velocity is:

$$v(t) = \frac{1.17\beta e^{-\omega_0 t}}{\sqrt{1 - e^{-\omega_0 t}}}\boldsymbol{H}(t) . \quad (2.17)$$

Analysis of the expression (2.17) provides the following features of the rupture velocity in this model:

– velocity is a monotonically decreasing function of time (hypocentral distance);
– rupture velocity is singular at $t = 0$; for

$$t \ll 1 \quad v(t) \cong \frac{1.17\beta}{\sqrt{\omega_0 t}} .$$

2.5. *Algorithm for time-series prediction*

Suppose that at a given site we have observations $U_j(t)$, $j = 1, ..., N$ of N small earthquakes originating within the rupture area of an anticipated large earthquake. We assume that these earthquakes have the same focal mechanism as the large event. If the observations cover the anticipated main event rupture area, we try to simulate the large earthquake as the sum of subevents generated from the properly scaled and lagged observed small earthquakes. Meanwhile we account for the source-receiver geometry by choosing only those subevents that are co-located with the main event. We account for directivity effects by determining rupture times of subevents according to both their position on the fault with respect to the main event hypocenter and their azimuth between the site and the direction of rupture propagation.

We can not apply the results of section 2.2. directly to the observed set of small earthquakes because of three major difficulties: i) the number of observations is usually small; ii) they are distributed non-uniformly between the hypocenter and the boundary of the anticipated rupture area; and iii) they have different sizes. The following simple procedure allows to overcome the first two problems. We choose a new number of subevents N_0 that is assumed to be sufficiently large to mimic a continuous uniform distribution of subevents on the fault. Testing on data shows that $N_0 = 100$ works quite well (see below). Then we uniformly distribute N_0 subevents on the fault, for example, by assigning

$$R_j = \frac{j}{N_0} R_0 ,$$

where R_j is the distance between the hypocenter of the main event and the j-th subevent, and R_0 denotes the size of the main event. Now we take the observed small earthquake closest to the main event's hypocenter. All subevents located closer to the main event's hypocenter than this small earthquake are assumed to have waveforms similar to that from this observed small earthquake. Subevents positioned further than the first observed small earthquake but closer than the second from the origin small earthquake are assumed to be similar to the latter one, etc. This procedure divides the whole set of N_0 subevents into n_1 subevents similar to the observed small earthquake closest to the main event's hypocenter, n_2 subevents similar to the second closest observed earthquake, etc. Thus after arranging the observed small earthquakes according to their distances to the main event's hypocenter, the numbers $n_1, n_2, ..., n_N$ are proportional to the difference between hypocentral distances of two successive small earthquakes. There are many other possible ways to take care of (i) and (ii), in particular in a more accurate manner accounting for the source-receiver geometry, and/or making $n_1 = n_2 = ... = n_N$.

If subevents' corner frequencies are sufficiently large, we can use the limiting case $\omega_{0e} = \infty$ of (2.7) to determine their rupture times. Note that in the case of a large number of similar small subevents our considerations show that

$$\sigma_j \approx \frac{1}{N} \frac{M_0}{M_{0e}} .$$

Alternatively, the coefficients σ_j in the basic relation (1.8) can be found as a solution to a linear least squares problem (1.7). The resulting algorithm for time-series prediction, based on this approach, has the following steps:

1) estimate the total rupture duration T_0 by dividing the fault size R_0 by the average rup-

ture velocity υ (*e.g.*, $\upsilon = 0.85\,\beta$). Calculate the target corner frequency $\omega_0 = 2\pi/T_0$;

2) determine the apparent source corner frequency $\omega_{0\theta}$ at the site according to the directivity factor D:

$$\omega_{0\theta} = \frac{\omega_0}{1 - \frac{\upsilon}{\beta}\cos\theta}$$

(relation (1.10)).

3) calculate the seismic moment M_{0j} (or estimate moments from the catalog magnitudes) for each observed subevent;

4) determine the rupture time τ_j of the jth subevent by solving (2.7) with $\omega_{0e} = \infty$:

$$\rho_j = 1 - \left[1 + \omega_{0\theta}\,\tau_j\right] e^{-\omega_{0\theta}\tau_j}$$

where ρ_j is the distance between the main shock's and subevent's hypocenters normalized by the size R_0 of the main fault plane (*e.g.*, $\rho_j = 1/j$);

5) determine coefficients σ_j. This can be done, for example, by adjusting subevents to a common seismic moment M_0/N_0, then

$$\sigma_j = \frac{1}{N_0}\,\frac{M_0}{M_{0j}};$$

or, more naturally, use the same normalization $\sigma_j = \sigma$ of the stress drop for all subevents:

$$\sigma = \frac{M_0}{n_1 M_{01} + n_2 M_{02} + \ldots + n_N M_{0N}};$$

6) add observed subevents' waveforms according to (1.8).

We would like to emphasize once again that this algorithm requires only the seismic moment of each subevents.

3. Spectral prediction

In this section we suggest an alternative approach to ground motion prediction. We consider only the amplitude spectra. Fourier amplitude spectrum is a measure of ground motion that (i) is related to both the earthquake source and propagation/site effects; (ii) covers the entire seismic bandwidth; (iii) directly applies to earthquake engineering; and (iv) is a robust measure of the total ground motion. At the same time phase spectra carry the most uncertainty and variability, being influenced by details of the rupture nucleation and propagation, size and location of asperities, etc.

First we consider the problem of normalization of small earthquakes spectra in the empirical Green's function method. Joyner and Boore (1986) considered the case of a number of identical subevents with uniformly distributed rupture times (see also Heaton and Hartzell, 1989). We generalize their results for an arbitrary distribution of small earthquakes by using a slightly different approach that is based on a direct comparison of levels of the target and added spectra at the lowest and the highest frequencies. The goals of this part of the paper are (i) to present a general method of normalization of subevents' amplitude spectra to match both the low- and high-frequency levels of the target spectrum, and (ii) to propose a new method of adding subevents' spectra together based on a new notion of partial coherence.

By «spectral normalization» we mean multiplication of each spectrum by a constant that depends only on the subevent's size. This normalization is equivalent to simply changing the corresponding seismic moment (or stress drop). Thus we do not change the shape of the spectrum by applying a filter in the spectral domain.

Recently, we have shown (Tumarkin *et al.*, 1994), that no matter what the distribution of subevents is, it is impossible to produce a target spectrum without prior scaling of events' waveforms unless there is a relation $\gamma = \delta/2$ between the source spectral falloff γ and the seismic moment's scaling exponent δ (such that $M_0\,\omega_0^{\delta} = \text{const}$ for a seismic moment M_0 and a corner frequency ω_0). Therefore in order to match a target spectrum by adding a given distribution of subevents we are left with an alternative: 1) normalize subevents spectra with-

out altering their distribution; and 2) normalize subevents spectra and their distribution. The latter possibility corresponds to Joyner and Boore (1986).

In Joyner-Boore's method η identical small earthquakes are added together and their waveforms (*i.e.* spectra) scaled by a constant ν. Assuming a constant rupture velocity, the rupture times of the subevents are uniformly distributed between 0 and the total rupture duration T. This procedure results in a coherent summation at lower frequencies (below the corner frequency ω_0 of the target spectrum) and incoherent summation at higher frequencies (above the common corner frequency ω_{0e} of subevents). Joyner and Boore (1986) established the relations to be satisfied by η and ν in order for the spectrum to match the target spectrum at the lowest and highest frequencies:

$$\eta = \left(\frac{\omega_0}{\omega_{0e}}\right)^{2\gamma}; \quad \nu = \left(\frac{\omega_0}{\omega_{0e}}\right)^{2\gamma-\delta} \tag{3.1}$$

In other words, the Joyner-Boore's procedure is the following: for a single subevent with corner frequency at ω_{0e} generate η subevents, similar to the given one, and multiply each by ν. Take these scaled subevents and add them with uniformly distributed time-delays.

We establish a necessary and sufficient condition (inequality (3.5) below) for producing a target spectrum using a given set of subevents without changing their distribution (*i.e.*, without generating additional subevents). On the other hand, it is always possible to fit the target spectrum by appropriately normalizing the distribution and scaling the spectra. We discuss the method in which each subevent's waveform should be scaled according to the simulated-to-subevent seismic moment ratio raised to a power. The value of this power $(1 - 2\gamma/\delta)$ depends only on the source spectral falloff γ and the scaling of seismic moment δ. Thus Joyner-Boore's results are extended to an arbitrary distribution of sizes of subevents.

The summation of subevents amplitude spectra is controlled by a frequency-dependent partial coherence exponent. This novel approach allows to avoid the deficit of the resulting spectral prediction in the vicinity of the target corner frequency.

3.1. *General relations*

Again we consider N subevents with seismic moments M_{01}, ..., M_{0N} and corner frequencies ω_1, ..., ω_N; M_0, and ω_0 are the seismic moment and the corner frequency of the target event; and γ is the common spectral falloff.

The following results are based on the seismic moment scaling assumption:

$$M_{0e}\,\omega_{0e}^{\delta} = C_M \tag{3.2}$$

where C_M is a constant independent of M_{0e}, ω_{0e}; and δ is the seismic moment scaling exponent. For the constant stress drop seismic moment scaling $\delta = 3$ (Kanamori and Anderson, 1975).

We now obtain general relations between major characteristics of the model – seismic moment scaling exponent δ, spectral falloff γ, and subevents corner frequency distribution – that result from conditions of matching the target spectrum at lowest and highest frequencies (*cf.*, Tumarkin *et al.*, 1994). Prior to adding subevents, each spectrum is normalized by a constant σ_j. As pointed out earlier, this is equivalent to multiplying the seismic moment (or stress drop) by σ_j.

Let us now assume that at low frequencies the subevent spectra add coherently. This is equivalent to the natural assumption that the seismic moment of the simulated event M_0 is the sum of seismic moments of normalized subevents. Using (3.2) we find:

$$M_0 = M_{01} + M_{02} \ldots + M_{0N} =$$

$$= C_M(\sigma_1\,\omega_1^{-\delta} + \sigma_2\,\omega_2^{-\delta} \ldots + \sigma_N\,\omega_N^{-\delta}). \tag{3.3}$$

Next consider summation of subevent spectra for frequencies above the highest corner

frequency of subevents. For the $\omega^{-\gamma}$-model (1.5) the high-frequency source spectral level at any frequency ω above the corner frequency ω_{0e} is $C_S M_{0e} \omega_{0e}^{\gamma} \omega^{-\gamma}$. Assuming that the high-frequency energy of the main event is the incoherent sum of the energy of all subevents, we find (*cf.*, Joyner and Boore, 1986; Frankel, 1991; Tumarkin *et al.*, 1994):

$$C_S^2 M_0^2 \omega_0^{2\gamma} \omega^{-2\gamma} =$$

$$C_S^2(\sigma_1^2 M_{01}^2 \omega_1^{2\gamma} + \sigma_2^2 M_{02}^2 \omega_2^{2\gamma} + \ldots + \sigma_N^2 M_{0N}^2 \omega_N^{2\gamma}) \omega^{-2\gamma}$$

Thus,

$$M_0^2 = C_M^2 \omega_0^{-2\gamma}(\sigma_1^2 \omega_1^{2\gamma-2\delta} + \sigma_2^2 \omega_2^{2\gamma-2\delta} + \ldots + \sigma_N^2 \omega_N^{2\gamma-2\delta}). \tag{3.4}$$

In the next section we establish a necessary and sufficient condition for existence of multipliers σ_j satisfying the eqs. (3.3) and (3.4).

3.2. *A criterion for the possibility of normalization*

Quite unexpectedly, the general relations (3.3)-(3.4) imply a very strong condition for existence of normalizing constants σ_j. Roughly, this condition means that the total moment of the given distribution of events is large enough to satisfy an inequality for a new functional on the distribution, introduced below.

Let us consider the relation (3.3). Taking squares of both sides of the eq. (3.3) and applying the Cauchy inequality

$$\left(\sum x_j y_j\right)^2 \le \left(\sum x_j^2\right)\left(\sum y_j^2\right)$$

with $x_j = \sigma_j \omega_j^{\gamma-\delta}$ and $y_j = \omega_j^{-\gamma}$, we get:

$$M_0^2 = C_M^2(\sigma_1 \omega_1^{-\delta} + \sigma_2 \omega_2^{-\delta} \ldots + \sigma_N \omega_N^{-\delta})^2 \le$$

$$C_M^2(\sigma_1^2 \omega_1^{2\gamma-2\delta} + \sigma_2^2 \omega_2^{2\gamma-2\delta} + \ldots + \sigma_N^2 \omega_N^{2\gamma-2\delta}) \cdot$$

$$(\omega_1^{-2\gamma} + \omega_2^{-2\gamma} + \ldots + \omega_N^{-2\gamma})$$

Comparing the last inequality with (3.3), we conclude that

$$\omega_1^{-2\gamma} + \omega_2^{-2\gamma} + \ldots + \omega_N^{-2\gamma} \ge \omega_0^{-2\gamma}. \tag{3.5}$$

This inequality (3.5) represents a necessary and sufficient condition for the given distribution of subevents to be able to produce the spectrum with the target corner frequency ω_0. In particular, for N identical subevents with the corner frequency ω_{0e} relation (3.5) implies that

$$N \ge \left(\frac{\omega_{0e}}{\omega_0}\right)^{2\gamma}.$$

Thus (3.5) can be a used as a constraint for the minimum number of summands (*i.e.*, the maximum size of the cell) in the kinematic rupture models using empirical Green's functions (Hutchings, 1994). For $\gamma > 1$ the inequality (3.5) indicates that the total area of subevents is greater than the area of the main event. For the particular case of a constant stress drop composite earthquake model this fact was observed in (Tumarkin *et al.*, 1994).

A violation of the condition (3.5) implies that *no matter how* we normalized the subevents' spectra, we would *never* be able to match both the low- and high-frequency levels of the target spectrum. On the other hand, if (3.5) is satisfied as a strict inequality, there is a wide choice of possible normalizing constants σ_j.

In the case of equality in (3.5) (equality in the Cauchy inequality) it follows that $x_j = \sigma_j \omega_j^{\gamma-\delta}$ and $y_j = \omega_j^{-\gamma}$ should be proportional. Therefore, the normalizing constants σ_j are *unique*: $\sigma_j = (\omega_0 / \omega_j)^{2\gamma-\delta}$.

It is worth noting that the condition (3.5) does not depend on the seismic moment scaling exponent δ but only on the distribution of subevents' corner frequencies and the spectral falloff γ.

3.3. *Partial coherence*

From the results of the preceding section we know that if the distribution of sizes of subevents was such that (3.5) became an equality, the choice of the normalizing constants σ_j would be unambiguous. Thus in a general situation we can normalize the distribution of subevents so that (3.5) becomes the equality by taking each subevent C times, where

$$C = \frac{\omega_0^{-2\gamma}}{\omega_1^{-2\gamma} + \omega_2^{-2\gamma} + \ldots + \omega_N^{-2\gamma}}$$

and normalize all subevents by $(\omega_0/\omega_j)^{2\gamma-\delta}$. This procedure will result in a simultaneous fit to the lowest and highest frequencies by satisfying both relations (3.3) and (3.4). That leaves us with the major problem of adding subevents in the intermediate frequency range.

Let us first write down two relations between the target $S_0(\omega)$ and subevents' $S_j(\omega)$ spectra which led to (3.3) and (3.4). At the lowest frequencies we have coherent summation:

$$|S_0(\omega)| = |S_1(\omega)| + |S_2(\omega)| + \ldots + |S_N(\omega)|$$

while at the highest frequencies we have incoherent summation:

$$|S_0(\omega)|^2 = |S_1(\omega)|^2 + |S_2(\omega)|^2 + \ldots + |S_N(\omega)|^2$$

We can rewrite these two relations in a uniform manner by introducing an exponent $\varepsilon(\omega)$ that determines the power to which each subevent spectrum should be raised before being added together. The value $\varepsilon(\omega) = 1$ corresponds to the coherent summation, and $\varepsilon(\omega) = 2$ corresponds to the incoherent summation. Thus

$$|S_0(\omega)|^{\varepsilon(\omega)} = |S_1(\omega)|^{\varepsilon(\omega)} + |S_2(\omega)|^{\varepsilon(\omega)} + \ldots + |S_N(\omega)|^{\varepsilon(\omega)}$$

If we assume that the radiation pattern of subevents abruptly changes from being perfectly coherent below the target corner frequency ω_0 to being perfectly incoherent above ω_0, that is introducing a step function $\varepsilon(\omega)$:

$$\varepsilon(\omega) = \begin{cases} 1, & \omega < \omega_0 \\ 2, & \omega > \omega_0 \end{cases},$$

we will get qualitatively the same result as Joyner and Boore (1986, 1988), namely, a gross underestimation of the target spectrum between the target corner frequency and the corner frequency of the largest subevent (fig. 2a,b).

To deal with this problem we introduce a gradual transition from perfect coherence to perfect incoherence in the intermediate frequency range (fig. 7a). Using an analogy to the theory of optics we call this transition frequency interval «a partial coherency» range.

The partial coherence exponent can be explicitly calculated in the case of identical subevents from the condition that subevents add to a perfect fit to the target spectrum. Using (1.5) and (3.1) we find:

$$\left\{\eta\left[\frac{\nu C_s M_{0e}}{\left(1+\left(\frac{\omega}{\omega_{0e}}\right)^2\right)^{\frac{\gamma}{2}}}\right]^{\varepsilon(\omega)}\right\}^{\frac{1}{\varepsilon(\omega)}} = \frac{C_S M_0}{\left(1+\left(\frac{\omega}{\omega_0}\right)^2\right)^{\frac{\gamma}{2}}},$$

from which we can solve for

$$\varepsilon(\omega) = \frac{1}{1 - \dfrac{\ln\left[1+\left(\frac{\omega}{\omega_0}\right)^2\right] - \ln\left[1+\left(\frac{\omega}{\omega_{0e}}\right)^2\right]}{4\ln\left(\frac{\omega_{0e}}{\omega_0}\right)}} \tag{3.6}$$

Note that this expression does not depend on either δ or γ.

For a distribution of subevents we have a distribution of corner frequencies. Although we can use any of these corner frequencies, we determine $\varepsilon(\omega)$ using the smallest ω_{0e} corresponding to the largest subevent. By the defini-

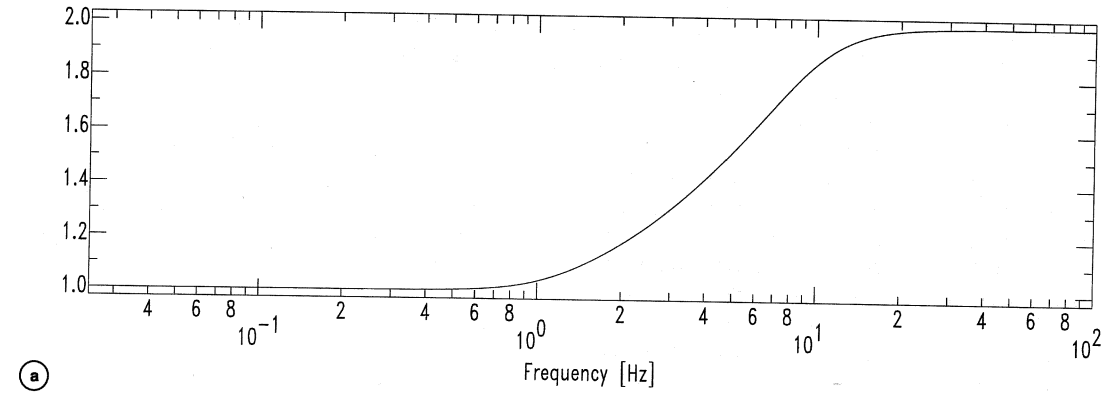

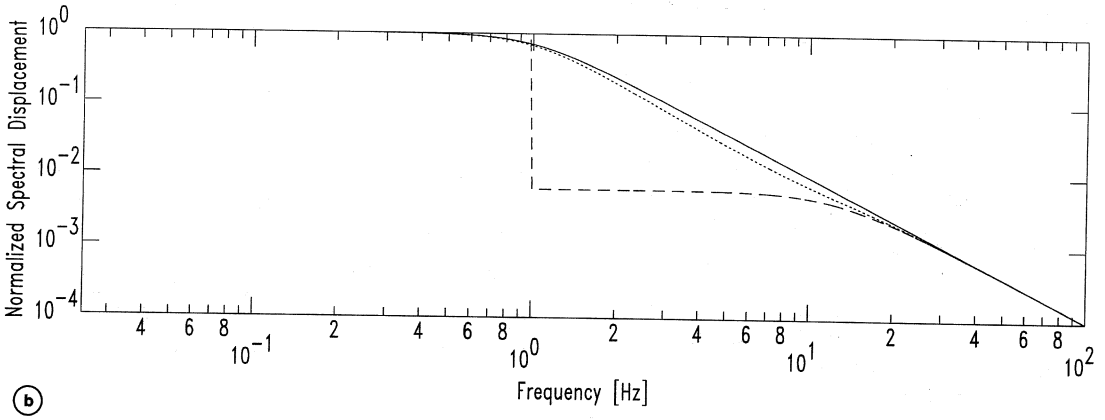

Fig. 7a,b. a) Partial coherence exponent $\varepsilon(f)$, determined by the expression (3.6) with $f_0 = 1$ Hz and $f_{0\varepsilon} = 10$ Hz; b) simulation of the Brune's amplitude spectrum ($f_0 = 1$ Hz) (solid line) by a fractal distribution of subevents with $D = 2$ and corner frequencies of subevents between 10 Hz and 25 Hz assuming an abrupt change of radiation pattern of subevents from a perfect coherence below f_0 to a perfect incoherence above f_0 (dashed line); after introducing partial coherence exponent (3.6) (dotted line).

tion of $\varepsilon(\omega)$ the fit to a target spectrum would be perfect had we used a single subevent as in Joyner-Boore's original method. In a general situation the error due to such approximation is not very significant (fig. 7b); we account for 75% of the energy.

3.4. *Algorithm for spectral prediction*

In this section we summarize the results of previous sections that describe a new general algorithm for empirical spectral prediction (Archuleta and Tumarkin, 1993). This approach utilizes only amplitude spectra of subevents, thus it does not require any phase information (such as location of the hypocenter, time delays between subevents, etc.).

Suppose that at a given site you have N records of earthquakes, located within the prospective rupture area of a large earthquake with the seismic moment M_0 and the corner frequency ω_0. The idea of the algorithm, common for all EGFM approaches, is that the ob-

served records already contain information on the propagation path from the simulated source to the studied station and on the local geology beneath the station. Moreover, if there is a way to use as many recorded events, as possible, then the possible dependence of the simulated spectrum on peculiarities of a single record is significantly reduced. Also, different path effects are taken into account by spanning a majority of the anticipated fault plane. This is especially important in case of larger earthquakes where rupture lengths of tens kilometers are comparable to the distance between source and site.

The proposed algorithm includes the following steps:

1) Calculate the seismic moment M_{0j}; S-wave corner frequency ω_j; and the source spectral falloff γ for each jth subevent. This can be done, for example, on the basis of existing automated methods of fitting observed spectra (*e.g.*, Fletcher and Boatwright, 1991; Lindley and Archuleta, 1992).

2) Determine the scaling exponent δ for the seismic moment. This is done by applying regression analysis to logarithms of values of the seismic moment and of corner frequencies, calculated in step (1).

3) Determine the apparent source corner frequency $\omega_{0\theta}$ at the site according to the directivity factor D controlled by the azimuth θ from the rupture direction to the given site:

$$\omega_{0\theta} = \frac{\omega_0}{1 - \frac{v}{\beta}\cos\theta}$$

(relation (1.10)).

4) Multiply each observed amplitude spectrum $|U_j(\omega)|$ by $(\omega_{0\theta}/\omega_j)^{2\gamma-\delta}$:

$$|\tilde{U}_j(\omega)| = \left(\frac{\omega_{0\theta}}{\omega_j}\right)^{2\gamma-\delta} |U_j(\omega)|$$

5) Calculate the normalizing constant C for the observed distribution of subevents:

$$C = \frac{\omega_{0\theta}^{-2\gamma}}{\omega_1^{-2\gamma} + \omega_2^{-2\gamma} + \ldots + \omega_N^{-2\gamma}}$$

6) Determine the partial coherence exponent $\varepsilon(\omega)$:

$$\varepsilon(\omega) = \frac{1}{1 - \frac{\ln\left[1 + \left(\frac{\omega}{\omega_{0\theta}}\right)^2\right] - \ln\left[1 + \left(\frac{\omega}{\omega_{\min}}\right)^2\right]}{4\ln\left(\frac{\omega_{\min}}{\omega_{0\theta}}\right)}}$$

where $\omega_{\min}$ is the smallest corner frequency of subevents, *i.e.*, the corner frequency of the largest subevent.

7) Raise the normalized amplitude spectra $|\tilde{U}_j(\omega)|$ to the power $\varepsilon(\omega)$ and add them together, taking each normalized spectrum C times. The resulting spectral prediction $|U_0(\omega)|$ is expressed by:

$$|U_0(\omega)| = C^{\frac{1}{\varepsilon(\omega)}} \left\{ |\tilde{U}_1(\omega)|^{\varepsilon(\omega)} + |\tilde{U}_2(\omega)|^{\varepsilon(\omega)} + \ldots + |\tilde{U}_N(\omega)|^{\varepsilon(\omega)} \right\}^{\frac{1}{\varepsilon(\omega)}}.$$

8) Scale the resulting spectrum $|U_0(\omega)|$, acconting for a possible difference between the average stress drop of subevents and the stress drop of predicted main event. Technically this is achieved by comparing the given value of the seismic moment M_0 for the simulated event with the result of extrapolation of the regression relation, obtained in step 2, to the value $\omega_{0\theta}$ of the apparent source corner frequency. The ratio between the target and extrapolated seismic moments gives the scaling multiplier

to be applied to predicted spectrum $U_0(\omega)$, accounting for the difference in stress drops.

4. Testing on data

We have tested the time series and spectral algorithms on data from the Joshua Tree earthquake sequence. Results from a retrospective «prediction» of the M_W 6.1 Joshua Tree mainshock using 5 smaller earthquakes (table I) are presented. The source parameters of the used subevents were taken from (Lindley, 1994). In order to obtain *S*-wave corner frequencies we divided *P*-wave corner frequencies from table I by $\sqrt{3}$. For example, for the main event we get $f_0 = 0.29$ Hz. The main event is almost purely strike-slip rupture with a roughly 12 km square fault-plane striking N10°W. For a rupture velocity 3 km/s that would imply a total rupture duration of 4 s and the source corner frequency 0.25 Hz, which is consistent with the above mentioned value. The rupture propagated unilaterally from the hypocenter to the North (Kanamori *et al.*, 1993).

The studied site is the Garner Valley Downhole Array (GVDA) (Archuleta *et al.*, 1992, Archuleta and Tumarkin, 1993) located at an epicentral distance of 45 km and an azimuth 226° from the mainshock. Therefore the angle θ for calculating the directivity factor is 124°. Consequently $D = 0.68$ assuming $\upsilon = 0.85\,\beta$. We used digital acceleration records from the downhole three-component, dual-gain kinemetrics force balance accelerometer, located 220 m below the surface in a competent rock (shear wave velocity 3.15 km/s), and from a similar surface instrument. Upper 18 m are comprised of recent alluvial deposits forming a lakebed valley (shear wave velocity between 280 and 90 m/s) (Archuleta *et al.*, 1992). The water table is about 1 m (during winter rainy season it reaches the surface). Thus we can test the performance of the algorithms applied to a rock site and a soft soil liquefiable site.

We first show the time-series predictions

Table I. Source parameters of the Joshua Tree earthquake sequence. Listed are the main event and 5 subevents, used in the present study.

Earthquake	Latitude N (degrees min)	Longitude W (degrees min)	Depth (km)	Distance[#] (km)	M_L	Seismic moment (dyne-cm)	*P*-wave corner frequency (Hz)	Stress drop (bars)
4/23 02:25:30	33 57.37	116 19.05	11.5	1.0	4.6	$1.2\ 10^{23}$	1.47	31
4/23 04:50:23	33 57.67	116 19.05	12.38	0.0	6.1	$1.9\ 10^{25}$	0.51	203
4/23 18:56:03	33 59 47	116 17.06	3.49	10.1	4.4	$3.1\ 10^{22}$	1.91	17
4/26 03:07:58	33 59.59	116 19.94	8.73	5.3	3.6	$7.9\ 10^{21}$	3.17	20
5/02 12:46:41	33 59.36	116 17.21	3.97	9.5	4.2	$2.6\ 10^{22}$	2.69	41
5/17 06:21:32	33 57.60	116 18.97	9.44	2.9	3.3	$1.9\ 10^{21}$	4.78	17

Earthquake locations are taken from the Caltech catalog. The seismic moment of the Joshua Tree main shock is taken from (Kanamori *et al.*, 1993). Seismic moments and *P*-wave corner frequencies of earthquakes were then determined by the spectral ratio method by Lindley (1994). The ratio of *P*-wave to *S*-wave corner frequencies is assumed to be $\sqrt{3}$.

[#] Distance is measured between the hypocenters of the main event and the aftershock.

using the algorithm with a constant stress drop scaling from section 2.5. We rearrange small earthquakes according to their distances 1, 2.9, 5.3, 9.5, 10.1 km from the mainshock's hypocenter (table I). Having only 5 subevents and consequently only 5 time-delays will provide a very poor fit to the target source function. Thus we have taken 100 subevents uniformly located at hypocentral distances 0-12 km, *i.e.*, $\rho_j = j/100$, $j = 1, ..., 100$. As discussed in section 2.5. for subevents located at less than 1 km we assume that their waveforms are similar to the small earthquake closest to the mainshock's hypocenter (M_L 4.6 foreshock), subevents positioned between 1 and 2.9 km are assumed to be similar to the second from the origin small earthquake (M_L 3.3 aftershock), etc. The simulated time series are shown in fig. 8.

Although there is a scatter in the seismic moment scaling for subevents, it is reasonably well described by the value $\delta = 3$. The source spectral falloff γ was assumed to be 2 (Lindley, 1994). At the same time the stress drop of the Joshua Tree main shock was approximately 10 times greater than its aftershocks (Kanamori *et al.*, 1993; Lindley, 1994). By multiplying the main event corner frequency by the directivity factor 0.68 we are already producing a seismic moment that is $0.68^{-3} = 3.3$ times larger. Therefore to account for the difference between the stress drops of the main event and subevents we need to multiply our predictions

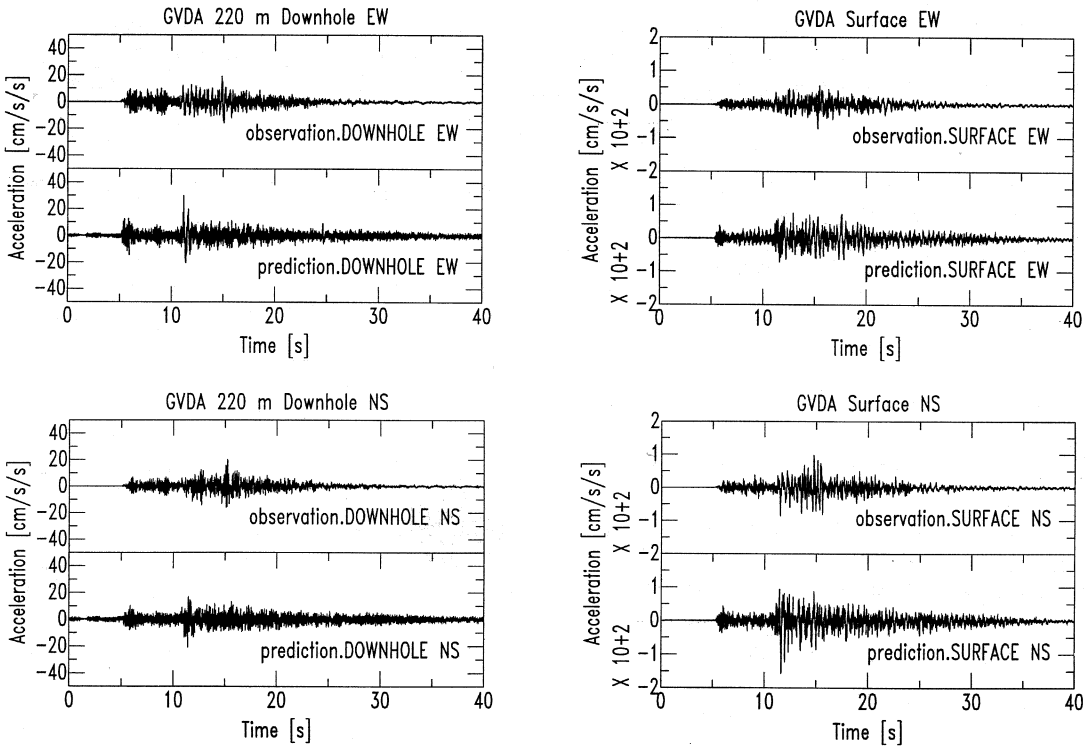

Fig. 8. Time-series prediction of the Joshua Tree mainshock at the 220 m downhole and surface GVDA accelerographs. Top traces are observed mainshock waveforms, bottom traces are simulations by the algorithm described in section 2.5. Time-series were lowpassed below 25 Hz.

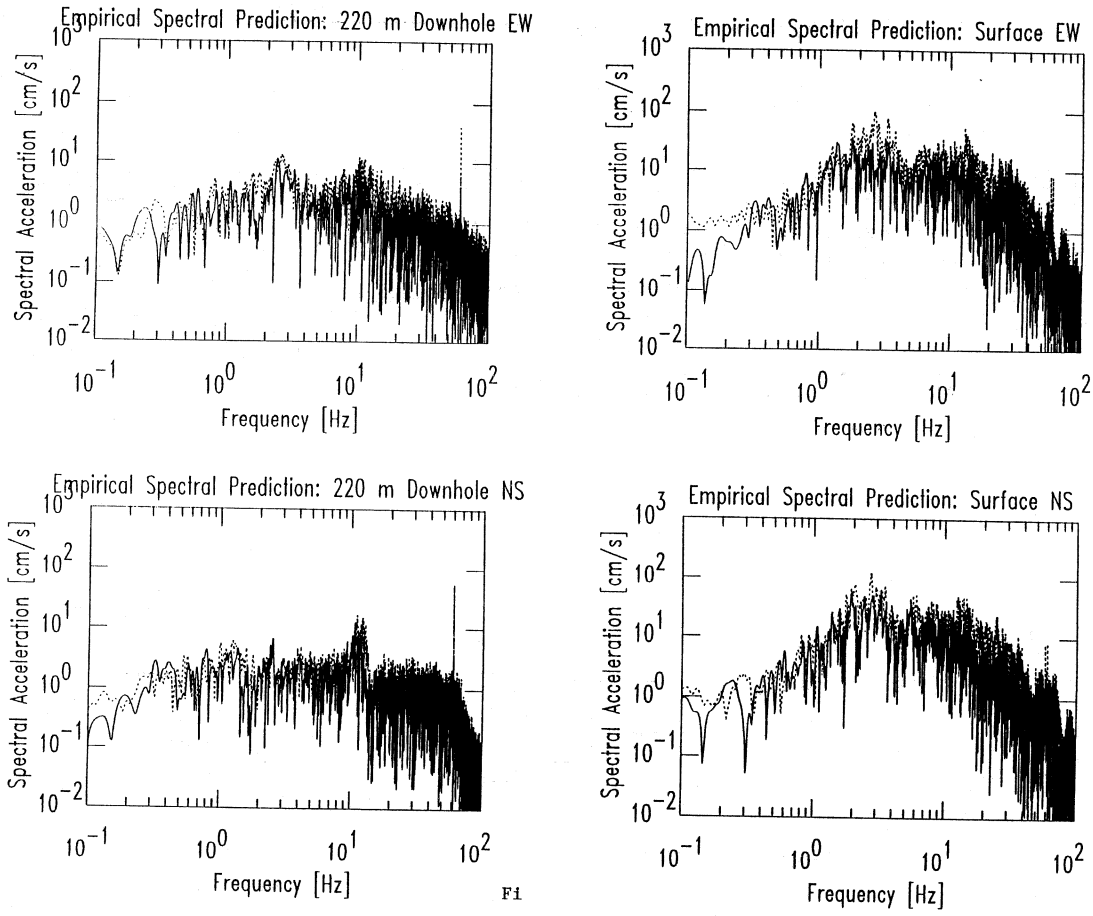

Fig. 9. Empirical spectral prediction of the Joshua Tree mainshock at the 220 m downhole and surface GVDA accelerographs. Observed mainshock Fourier amplitude spectra are plotted as solid lines, simulations by the algorithm described in section 3.4. are dotted lines.

from step 6 of section 3.4. by an additional factor of 3 (step 8). Figure 9 shows comparisons of predicted whole record amplitude spectra with observations.

Using random vibration theory (*e.g.*, Joyner and Boore, 1988) we obtain estimates of the response spectrum from the Fourier amplitude spectrum without using any phase information. The only additional parameter needed for such an estimate is the duration of the record. The shorter the duration used for such an estimate, the higher the predicted response spectrum. The explanation is simple: releasing the same amount of energy (as the amplitude spectrum is preserved) in a shorter time produces higher amplitudes of the signal. Thus the underestimation of the duration in this approach will result in an overestimation of the response spectrum. For the duration we used the value 12 s, which corresponds to the average Trifunac-Brady duration (Trifunac and Brady, 1975) of downhole and surface horizontal components of acceleration. For a forward prediction it is possible to use an empirical estimate of the duration T in

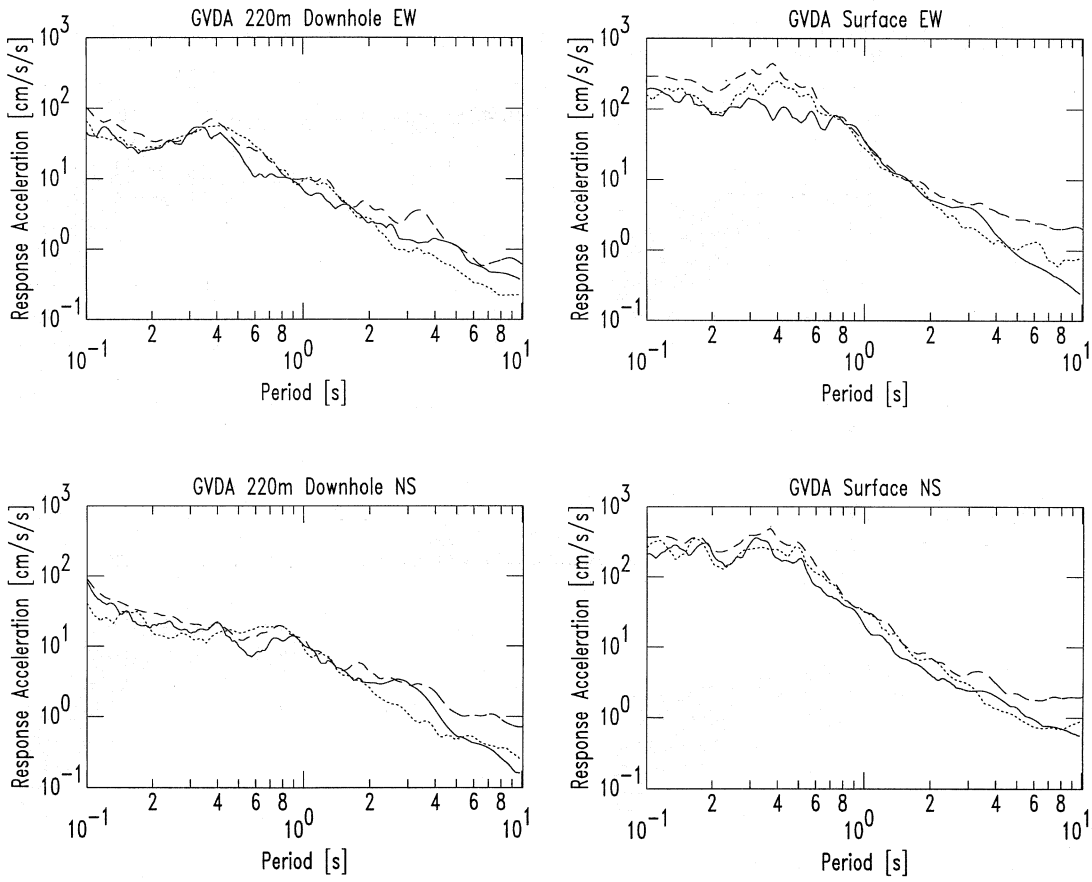

Fig. 10. Prediction of the 5%-damping acceleration response spectra from the Joshua Tree mainshock at the 220 m downhole and surface GVDA accelerographs. Observed response spectra are plotted as solid lines, response spectra corresponding to time-series predictions (fig. 8) are dotted lines. Estimates obtained by the random vibration method from the ESP predictions (fig. 9) are dashed lines.

terms of the earthquake's corner frequency f_0 and epicentral distance r, *e.g.*, $T = 1/f_0 + 0.05\ r$ (Joyner and Boore, 1988).

Comparisons of observed response spectra (solid lines) with predictions obtained from time-series (dotted lines) and spectral (dashed lines) methods are shown in fig. 10. The overall quality of predictions by the both the time-domain and spectral approaches is very good, although the spectral method tends to slightly overestimate observed spectral ordinates at longer periods.

5. Discussion

We have presented two new approaches – time domain and spectral domain – to empirical ground motion prediction. Our results apply to the problem of modeling large earthquakes as multiple events.

Extending the idea of Wennerberg (1990) we have developed a method for adding identical small subevents to match seismic radiation from a large earthquake over the whole frequency range from the lowest to the highest

frequencies. In this method the position of a subevent on the fault plane of the simulated large event uniquely determines the subevent's rupture time. We corrected the negative rupture times in the Wennerberg's model of a linear rupture and have extended the analysis to a circular rupture model (a different rupture geometry, *e.g.* expanding elliptical rupture, can be treated analogously). We also considered a fault consisting of Boatwright's asperities.

Our results have interesting applications to modeling of earthquake sources although the circular faulting models introduced in this paper are not supposed to describe a realistic earthquake rupture process. Let us discuss some obvious shortcomings of these models. First the initial rupture velocity is always supershear. Second the rise time over the fault is constant and is equal to the duration of the subevent. Consequently for a fault composed of infinitely small Brune's cracks the rise time everywhere on the fault is zero but the rupture velocity at the origin is finite. It turns out that the rupture decelerates from the value 1.65 β at the origin to 0 at the boundary with an average value of the rupture velocity of 0.85 β. The average rupture velocity remarkably coincides with the rupture velocity for the dynamic self-similar circular rupture (Kostrov, 1964). The rupture velocity for a similar fault composed of infinitely small Boatwright's asperities has a singularity at the origin.

At the same time for a fault composed of finite subsources the rise time is not zero but the rupture velocity at the origin is infinite. Indeed at time zero we have an instantaneous rupture of a finite area occupied by the first subevent. This is common for numerical models of spontaneous rupture where some critical distance of rupture nucleation is required (Andrews, 1976; Day, 1982; Harris and Day, 1993). The stress must be released over a finite area in order to drive the rest of the fault. Until there is a better understanding of the nucleation process of an earthquake, we do not want to overinterpret the physical nature of the circular ruptures.

The circular rupture introduced in section 2.3. does provide a kinematic description of a source with finite rupture velocity over a finite circular fault that produces a Brune pulse and the corresponding spectrum. This is very different from Brune's original faulting model (Brune, 1970) where the rupture velocity was infinite. Our considerations can be generalized to show that any source time function can be modeled as a non-instantaneous rupture of a homogeneous fault by choosing a specific variable rupture velocity.

As we pointed out earlier, the distribution of stress drops of subevents in a composite earthquake model uniquely determines the rupture velocity over the fault plane. The relation (2.3) shows that the converse is also true. At the same time (2.3) implies that a small-to-large earthquake transfer function $P(\omega)$ uniquely determines only the product of the functions $\tilde{\sigma}(\rho(t))$ and $\rho'(t)$. This fact means that there is a trade-off between rupture velocity and stress drop (or moment release) (Boore and Joyner, 1978; Joyner, 1991). For a linear rupture an increase in one of these parameters will imply a proportional decrease in the other one. Thus by performing source inversions using the empirical Green's function method (*e.g.*, Kanamori *et al.*, 1992) it is possible to determine only the product of the rupture velocity and the moment release at any moment of time. A similar problem was previously noticed in studies of more sophisticated models of earthquake sources (Madariaga, 1983; Spudich and Frazer, 1984). We have also established a necessary and sufficient condition (3.5) for the existence of a variable stress drop composite earthquake for any given set of subevents with uniformly distributed rupture times. In particular, the inequality (3.5) means that the total area of subevents should be greater than the area of the main event. For a constant stress drop composite earthquake model this fact was established in (Tumarkin *et al.*, 1994).

The rupture models used in this paper are based on an assumption that a subevent of a large seismic source can be described as a properly scaled and lagged small earthquake. They provide a simple and straightforward approach to utilizing observations of small earthquakes to predict ground motions from large earthquakes. On the other hand we outline two major problems associated with this hypothesis: singularity of the seismic moment release

density $\tilde{\sigma}(\rho)$ or the rupture velocity $\rho'(t)$ in (2.5), and the area paradox (3.5). Although the physical processes of large earthquake ruptures are still obscure, our results suggest that the high-frequency radiation from a subfault of a large rupture is different from the high-frequency radiation of an individual earthquake.

We have proposed a simple algorithm of the time-series prediction (section 2.5.) in which time delays between subevents are uniquely determined by their locations relative to the main shock hypocenter according to the specific rupture velocity in this model. This algorithm allows for any number of observed empirical Green's functions and requires only four input parameters for the simulated large event: i) target seismic moment M_0; ii) size of the rupture zone R_0; iii) location of the hypocenter; and iv) direction of rupture propagation. There are no other free parameters. By applying the method to all three components of ground motion we can predict simultaneously the three components of ground motion at a site. Thus the phase information between the vertical and horizontal components is tied together.

In the framework of the empirical Green's functions method we suggest an alternative approach to prediction of most important for the engineering practice site-specific characteristics. In essence it is possible to produce amplitude and response spectra without using the phase information at all. We have introduced a partial coherence exponent that controls the procedure of summation of subevents amplitude spectra in the entire frequency range. A constant rupture velocity imposes an abrupt transformation of the radiation pattern of subevents in the vicinity of the main event's corner frequency. Our partial coherence exponent allows for a gradual transition from a perfect coherence of subevents' radiation at the lowest frequencies to a perfect incoherency at highest frequencies.

This empirical spectral prediction approach, described in section 3.4., does not require the knowledge of details of seismic rupture and is theoretically capable of predicting ground motion spectra in the whole frequency range of analyzed subevents. The implementation of this algorithm is very efficient and straightforward.

6. Conclusions

We have developed and validated empirical ground motion prediction algorithms satisfying three critical conditions:

– the prediction is consistent with the entire observed seismic spectrum from the lowest to the highest frequencies;
– our source models incorporate the basic scaling relations between source parameters and spectral parameters;
– our methods allow for any subset of the available data, *i.e.*, for any number of recorded empirical Green's functions.

With these conditions met the ground motion prediction is internally self-consistent. It accounts for the complexity of the source while maintaining the basic seismic scaling relations and the complexity of the path/site effects without being dependent on the characteristics of a single empirical Green's function.

Our time-series prediction algorithm is based on determination of a non-uniform distribution of rupture times of subevents (Wennerberg, 1990). By introducing a specific rupture velocity we avoid the major problem of deficiency of predictions in the vicinity of the main event's corner frequency. This problem is an inherent feature of methods based on a uniform distribution of subevents' rupture times (Irikura, 1983; Joyner and Boore, 1986; Boatwright, 1988).

We have proposed a new alternative approach to the problem of simulation of a large earthquake by adding co-located subevents. By introducing a novel notion of a partial coherence we were able to sum subevents' amplitude spectra directly without using any information on their rupture times and phase histories. Predictions by this method are not dependent on details of the rupture nucleation and propagation, location of asperities and

other predominantly phase-affecting factors that are responsible for the most uncertainty of the time-domain methods.

Acknowledgements

The ideas were originated and critically reviewed in stimulating dialogues with Larry Hutchings. Grant Lindley provided source parameters of earthquakes used in this study. We are grateful to Raul Madariaga and an anonymous reviewer for critically reading the manuscript and providing helpful comments. We benefited from discussions with J. Anderson, J. Andrews, J. Boatwright, D. Boore, M. Çelebi, S. Day, K. Irikura, W. Joyner, C. Nicholson, P. Spudich, Y. Zeng. The work was supported by the National Science Foundation through Cooperative Agreement EAR-8920136 and USGS Cooperative Agreement 14-08-0001-A0899 to the Southern California Earthquake Center (SCEC), by the USGS grant No. 1434-94-G-2461, and by the Office of the Nuclear Regulatory Research, U.S. Nuclear Regulatory Commission Grant No. NRC-04-92-050 in cooperation with the Commissariat à l'Energie Atomique de France. SCEC publication No. 116. Institute for Crustal Studies contribution No. 0181-44EQ.

REFERENCES

AKI, K. (1967): Scaling law of seismic spectrum, *J. Geophys. Res.*, **72**, 1217-1231.

AKI, K. and P. G. RICHARDS (1980): *Quantitative Seismology. Theory and Methods.* vol. 1, 2 (W. H. Freeman and Company, San Francisco), pp. 932.

AKI, K. and K. IRIKURA (1991): Characterization and mapping of earthquake shaking for seismic zonation, in *Proceedings of the Fourth International Conference on Seismic Zonation*, vol. I (EERI, Oakland), 61-110.

ANDREWS, D. J. (1976): Rupture velocity of plane shear cracks, *J. Geophys. Res.*, **81**, 5679-5687.

ARCHULETA, R. J. and J. N. BRUNE (1975): Surface strong motion associated with stick-slip event in a foam rubber model of earthquakes, *Bull. Seismol. Soc. Am.*, **65**, 1059-1071.

ARCHULETA, R. J., S. H. SEALE, P. V. SANGAS, L. M. BAKER and S. T. SWAIN (1992): Garner Valley downhole array of accelerometers: instrumentation and preliminary data analysis, *Bull. Seismol. Soc. Am.*, **82**, 1592-1621 (Correction, *Bull. Seismol. Soc. Am.*, **83**, 2039, 1993).

ARCHULETA, R. J. and A. G. TUMARKIN (1993): Spectral modeling of composite earthquakes, *Seismol. Res. Lett.*, **64**, 29.

BENIOFF, H. (1955): Mechanism and strain characteristics of the White Wolf fault as indicated by the aftershock sequence, in *Earthquakes in California during 1955*, edited by G.B. OAKESHOTT (Calif. Div. Mines, Bull. 171), 199-202.

BEN-MENAHEM, A. (1961): Radiation of seismic surface-waves from finite moving sources, *Bull. Seismol. Soc. Am.*, **51**, 401-435.

BOATWRIGHT, J. (1988): The seismic radiation from composite models of faulting, *Bull. Seismol. Soc. Am.*, **78**, 489-508.

BOATWRIGHT, J. and D. M. BOORE (1982): Analysis of the ground accelerations radiated by the 1980 Livermore Valley earthquakes for directivity and dynamic source characteristics, *Bull. Seismol. Soc. Am.*, **72**, 1843-1865.

BOORE, D. M., and W. B. JOYNER (1978): The influence of rupture incoherence on seismic directivity, *Bull. Seismol. Soc. Am.*, **68**, 283-300.

BRUNE, J. (1970): Tectonic stress and the spectra of seismic shear waves from earthquakes, *J. Geophys. Res.*, **75**, 4997-5009 (correction, *J. Geophys. Res.*, **76**, 5002, 1971)

CHAEL, E. P. and R. P. KROMER (1988): Teleseismic time functions for large shallow subduction zone earthquakes, *Bull. Seismol. Soc. Am.*, **78**, 561-570.

DAN, K., T. WATANABE, K. TANAKA and R. SATO (1990): Stability of earthquake ground motion synthesized by using different small-event records as empirical Green's functions, *Bull. Seismol. Soc. Am.*, **80**, 1433-1455.

DAY, S.M. (1982): Three-dimensional simulation of spontaneous rupture: the effect of nonuniform prestress, *Bull. Seismol. Soc. Am.*, **72**, 1881-1902.

DOUGLAS, A., J. A. HUDSON and R.G. PEARCE (1988): Directivity and the Doppler effect, *Bull. Seismol. Soc. Am.*, **78**, 1367-1372.

FLETCHER, J. B. and J. BOATWRIGHT (1991): Source parameters of Loma Prieta aftershocks and wave propagation characteristics along the San Francisco Peninsula from a joint inversion of digital seismograms, *Bull. Seismol. Soc. Am.*, *81*, 1783-1812.

FRANKEL, A. (1991): High-frequency spectral falloff of earthquakes, fractal dimension of complex rupture *b* value, and the scaling of strength on faults, *J. Geophys. Res.*, **96**, 6291-6302.

HARRIS, R.A. and S.M. DAY (1993): Dynamics of fault interaction: parallel strike-slip faults, *J. Geophys. Res.*, **98**, 4461-4472.

HARTZELL, S. H. (1978): Earthquake aftershocks as Green's functions, *Geophys. Res. Lett.*, **5**, 1-4.

HEATON, T. H. and S. H. HARTZELL (1989): Estimation of strong ground motions from hypothetical earthquakes on the Cascadia subduction zone, Pacific Northwest, *PAGEOPH*, **129**, 131-201.

HUTCHINGS, L. (1994): Kinematic earthquake models and synthesized ground motion using empirical Green's functions, *Bull. Seismol. Soc. Am.*, **84**, 1028-1050.

IRIKURA, K. (1983): Semi-empirical estimation of strong ground motions during large earthquakes, *Bull. Disast. Prev. Res. Inst., Kyoto Univ.*, **33**, 63-104.

JOYNER, W.B. (1991): Directivity for nonuniform ruptures, *Bull. Seismol. Soc. Am.*, **81**, 1391-1395.

JOYNER, W.B. and D. M. BOORE (1986): On simulating large earthquakes by Green's-function addition of smaller earthquakes, in *Earthquake Source Mechanics*, edited by S. DAS, J. BOATWRIGHT and C.H. SCHOLZ (AGU, Geoph. monogr. 37, M. Ewing vol. 6), 269-274.

JOYNER, W.B. and D. M. BOORE (1988): Measurement, characterization, and prediction of strong ground motion, in *Earthquake Engineering and Soil Dynamics II - Recent Advances in Ground-Motion Evaluation*, edited by J.L. VON THUN (ASCE, NY), 43-102.

KANAMORI, H. and D. L. ANDERSON (1975): Theoretical basis of some empirical relations in seismology, *Bull. Seismol. Soc. Am.*, **65**, 1073-1096.

KANAMORI, H., H.-K. THIO, D. DREGER, E. HAUKSSON and T. HEATON (1992): Initial investigation of the Landers, California, earthquake of 28 June 1992 using TERRAscope, *Geophys. Res. Lett.*, **19**, 2267-2270.

KANAMORI, H., J. MORI, E. HAUKSSON, T.H. HEATON, L.H. HUTTON and L. M. JONES (1993): Determination of earthquake energy release and M_L using TERRAscope, *Bull. Seismol. Soc. Am.*, **83**, 330-346.

KOSTROV, B.V. (1964): Self-similar problems of propagation of shear cracks, *J. Appl. Math. Mech. (PMM)*, *28*, 1077-1087.

LINDLEY, G. T. (1994): Source parameters of the 23 April 1992 Joshua Tree, California, earthquake, its largest foreshock, and aftershocks, *Bull. Seismol. Soc. Am.*, **84**, 1051-1057.

LINDLEY, G.T. and R. J. ARCHULETA (1992): Earthquake source parameters and the frequency dependence of attenuation at Coalinga, Mammoth Lakes and the Santa Cruz Mountains, California, *J. Geophys. Res.*, **97**, 14137-14154.

MADARIAGA, R. (1983): High frequency radiation from dynamic earthquake fault models, *Ann. Geophys.*, **1**, 17-23.

PAPAGEORGIOU, A. and K. AKI (1983): A specific barrier model for the quantitative description of inhomogeneous faulting and the prediction of strong ground motion. Part I. Description of the model, *Bull. Seismol. Soc. Am.*, **73**, 693-722.

RANDALL, M. J. (1973): The spectral theory of seismic sources, *Bull. Seismol. Soc. Am.*, **63**, 1133-1144.

SOMMERVILLE, P.G. (1993): Engineering applications of strong ground motion simulation, *Tectonophysics*, **218**, 195-219.

SPUDICH, P. and L. N. FRAZER (1984): Use of ray theory to calculate high-frequency radiation from earthquake sources having spatially variable rupture velocity and stress, *Bull. Seismol. Soc. Am.*, **74**, 2061-2082.

TRIFUNAC, M.D. and A. G. BRADY (1975): A study of the duration of strong earthquake ground motions, *Bull. Seismol. Soc. Am.*, **65**, 581-626.

TUMARKIN, A.G., R.J. ARCHULETA and R. MADARIAGA (1994): Scaling relations for composite earthquake models, *Bull. Seismol. Soc. Am.*, **84**, 1279-1283.

WENNERBERG, L. (1990): Stochastic summation of empirical Green's functions, *Bull. Seismol. Soc. Am.*, **80**, 1418-1432.

WU, F. (1978): Prediction of strong ground motion using small earthquakes, in *Proceedings of the 2nd International Conference on Microzonation*, vol. II (San Francisco), 701-704.

ZENG, Y., J. G. ANDERSON and G. YU (1994): A composite source model for computing realistic synthetic strong ground motions, *Geophys. Res. Lett.*, **21**, 725-728.